https://doi.org/10.5194/egusphere-2024-592
Preprint. Discussion started: 15 April 2024
© Author(s) 2024. CC BY 4.0 License.

Haloturbation in the northern Atacama Desert revealed by a hidden subsurface network of calcium sulphate wedges

Aline Zinelabedin[1,2], Joel Mohren[1,3], Maria Wierzbicka-Wieczorek[1], Tibor J. Dunai[1], Stefan Heinze[4] Benedikt Ritter[1]

[1]Institute of Geology and Mineralogy, University of Cologne, Zülpicher Str. 49b, 50674 Cologne, Germany
[2]Institute of Geography, University of Cologne, Zülpicher Str. 45, 50674 Cologne, Germany
[3]Department of Geography, RWTH Aachen University, Wüllnerstr. 5b, 52062 Aachen, Germany
[4]Institute for Nuclear Physics, University of Cologne, Zülpicher Str. 77, 50937 Cologne, Germany

Correspondence to: Aline Zinelabedin (aline.zinelabedin@uni-koeln.de)

Abstract. While the formation of periglacial wedges and polygonal patterned grounds has been extensively studied and many of the processes involved have been understood, knowledge on the formation of similar post-sedimentary features found in arid to hyperarid environments remains largely rudimentary. Our contribution to fill this gap is the investigation of a network of vertically laminated calcium sulphate-rich wedges in the subsurface of the Aroma fan in the northern Atacama Desert. The subsurface wedges are characterised by high anhydrite contents and hence differ from the wedge and polygon structures of other study sites in the Atacama Desert, which appear to have been predominantly formed by thermal contraction or desiccation processes. By contrast, haloturbation mechanisms are thought to be a main driver of wedge formation at the Aroma fan site. Haloturbation requires moisture input, and hence Aroma fan wedge formation is likely to be associated with meteoric water received from sporadic rain events and episodes of arid climate characterised by slightly wetter conditions than prevailing at present. The polygonal patterned ground is covered by a stratigraphically younger gypsum-dominated surface crust cover. The presence of the surface crust could indicate an environmental change towards drier conditions, which favoured surface accumulation of calcium sulphate and other salts by means of atmospheric deposition. Such a climatic shift could have caused a deceleration of haloturbation and other wedge formation processes in the subsurface, although modern sediment conveyance from the surface towards its interior still appears to occur along cracks within the crust. In order to gain comprehensive insights into the complex mechanisms involved in wedge formation and formation rates, the establishment of a geochronological framework directly obtained from wedge and crust material remains indispensable. The temporal resolution of wedge growth stored within the succession of vertical laminae promises a high potential for the calcium sulphate wedges to be used as palaeoclimate archives, potentially helping to unravel wedge and polygonal patterned ground formation in other water-limited environments, such as Mars.

https://doi.org/10.5194/egusphere-2024-592
Preprint. Discussion started: 15 April 2024
© Author(s) 2024. CC BY 4.0 License.

1 Introduction

Geomorphological features such as subsurface wedges and polygonal patterned grounds are commonly found in periglacial environments (e.g. Lachenbruch, 1962; Washburn, 1956, 1979; Black 1976; Mackay, 1990) and have been successfully used as paleoclimate and paleoenvironmental archives (e.g. Williams, 1986; Liu and Lai, 2013; Opel et al. 2018; Campbell-Heaton et al., 2021). In general, wedge and polygon formation under periglacial conditions are driven by cryoturbation processes (Edelman et al., 1936). Water (both in liquid and solid state) is the main agent for ice wedge formation, as laminated periglacial ice wedge structures are caused by freeze-thaw cycles of ground ice (Edelman et al., 1936; Lachenbruch, 1962). Polygonal patterned ground is often indicative for the presence of subsurface wedge structures below the surface. The presence of similar polygonal patterns on the Martian surface has been observed by satellite imagery and correlated with the periglacial environment on Earth, with significant implications for the interpretation of geomorphology, surface processes, and water availability on Mars (e.g. Levy et al., 2010; Hauber et al., 2011; Soare et al., 2014; Amundson, 2018).

Strongly differing environmental conditions prevail in the arid to hyperarid Atacama Desert, where any landscape-sculpting processes are governed by an extreme water scarcity compared to a water-rich periglacial environment. However, polygonal patterned grounds associated with subsurface wedge structures very similar to periglacial ice wedge structures can also be found here (Ericksen, 1981, 1983; Allmendinger and González, 2010; Buck et al., 2006; Howell et al., 2006; Rech, et al., 2006; Howell 2009; Rech et al. 2019; Pfeiffer et al., 2021; Sager et al., 2021, 2022; Zinelabedin et al., 2022). In contrast to periglacial environments, polygonal patterned grounds and wedge structures in the Atacama Desert are not controlled and dominated by the interaction of ice and liquid water, suggesting that other processes are responsible for wedge-polygon-formation under hyperarid conditions. Several studies have proposed different formation processes for wedge structures and polygonal patterned grounds formed in such dry environments, including haloturbation (e.g. Buck et al. 2006; Ewing et al., 2006; Howell et al. 2006; Howell, 2009; Zinelabedin et al., 2022), thermal contraction (Yungay region; see Sager et al., 2021), and desiccation processes in playa-like environments (e.g. Atacama Desert; Ericksen, 1981, 1983; N-America; Neal et al. 1968). Key mechanisms of haloturbation are the dissolution and (re)precipitation of salt minerals in pore spaces leading to salt heave and rearrangement of deposits (e.g. Tucker, 1981; Fookes and Lee, 2018), as well as clast shattering. Direct precipitation of anhydrite from a solution results in the formation of the calcium sulphate polymorph β-anhydrite (β-$CaSO_4$; insoluble), which is thermodynamically stable (Tang et al., 2019; Beaugnon et al., 2020) and therefore occurs naturally in evaporite deposits (Beaugnon et al., 2020).

Another process known to cause swelling in the deposits is due to the phase transition ('gypsification') of the thermodynamically metastable and soluble γ-anhydrite (γ-$CaSO_4$; Tang et al., 2019; Beaugnon et al., 2020) over bassanite (hemihydrate; $CaSO_4{\bullet}0.5H_2O$) to gypsum ($CaSO_4{\bullet}2\ H_2O$), accompanied with a volume increase of ~61 % (Butscher et al., 2017, 2018; Jarzyna et al. 2021). The reversal process leads to a volume decrease of ~29 %

https://doi.org/10.5194/egusphere-2024-592
Preprint. Discussion started: 15 April 2024
© Author(s) 2024. CC BY 4.0 License.

for gypsum-bassanite transition (Milsch et al., 2011), and ~39 % of total volume decrease from gypsum to γ-anhydrite in an open system (Milsch et al., 2011; Sanzeni et al., 2016).

The fact that such processes can be identified in the hyperarid core of the Atacama Desert is linked to spatially widespread and persisting hyperarid conditions since at least the Early Miocene (Dunai et al., 2005; Evenstar et al. 2009; Jordan et al., 2014; Evenstar et al., 2017; Ritter et al., 2018, Ritter et al. 2022). Sporadic precipitation events have favoured extremely low erosion rates (Kober et al., 2007; Placzek et al., 2010, 2014; Starke et al., 2017; Mohren et al., 2020a, Ritter et al. 2023) resulting in long-term surface preservation (Dunai et al., 2005; Nishiizumi et al., 2005; Kober et al., 2007, Evenstar, et al., 2017; Ritter et al. 2019, 2022) and the accumulation of landscape-draping calcium sulphate-rich soil by atmospheric deposition (Ericksen, 1981, 1983; Rech et al., 2003; Michalski et al., 2004; Ewing et al., 2006; Wang et al., 2014, 2015; Rech et al., 2019). However, hyperaridity in the Atacama Desert is repeatedly interrupted by wetter but still (hyper-)arid conditions (e.g. Dunai et al. 2005; Jordan et al. 2014; Evenstar et al. 2017; Ritter et al., 2018, 2019, Diederich et al. 2020; Medialdea et al. 2020; Ritter et al. 2022, Wennrich et al., 2024), which appear to provide sufficient moisture to 'activate' salt dynamics in evaporite-bearing deposits (e.g. Buck et al., 2006; Howell et al., 2006; Howell, 2009; Wang et al., 2015; Rech et al. 2019).

Moisture input to the Atacama Desert is generally sourced from coastal fog (span. 'camanchaca'; see Cereceda et al. 2008) and sporadic rain events (recent precipitation events e.g. described in Bozkurt et al. 2016, Vicencio Veloso 2022, Cabré et al. 2022, Wennrich et al., 2024). Coastal fog is generated along the coastal cliff (Cereceda et al. 2008; Schween et al. 2020) by a persistent atmospheric inversion layer trapping moist Pacific air below ~1000 m a.s.l. (Houston, 2006; Garreaud et al. 2009). The maximum present-day fog altitude is ~1200 m a.s.l. (based on the fog-dependent spatial distribution of *Tillandsia landbeckii* sp.; Cereceda et al. 2008). The eastward migration of the coastal fog is limited by the high coastal cliffs, but it can cross the barrier through deep canyons (span. 'quebradas'; e.g. Río Loa, Tiliviche canyon). In an environment characterised by extreme water scarcity, the fog is considered to be one of the main agents for surface activity and modification in the hyperarid core of the Atacama Desert (Ericksen, 1981,1983; Rech et al., 2003). The probability of fog migration towards the hinterland decreases in eastern direction (del Río et al., 2018), such that the Central Depression or Precordillera receive little – if any – fog moisture. However, the atmospheric inversion layer has been found to have undergone vertical shifting on modern (del Río et al., 2018, Muñoz et al., 2016, Schween et al., 2020, Böhm et al., 2021) and Holocene (Latorre et al., 2011) timescales. These findings may be used as arguments for the assumption that a certain supply of remote inland surfaces with fog moisture could be achieved over the long term. Infrequent rain events occasionally approaching the inner Atacama Desert (e.g. Jordan et al., 2019) are usually caused by cut-off low pressure systems (Reyers et al., 2021), entering the Atacama Desert either from the north (see Böhm et al. 2021) or from the south (Stuut and Lamy, 2004).

https://doi.org/10.5194/egusphere-2024-592
Preprint. Discussion started: 15 April 2024
© Author(s) 2024. CC BY 4.0 License.

While such environmental conditions appear to favour the formation of polygonal patterned grounds and wedge structures, detailed analyses of the agents and processes causing wedge-polygon-formation in arid to hyperarid environments is still a matter of investigation. Furthermore, the timescales and environmental conditions under which the wedges form remain unresolved. Understanding (hyper-)arid wedge formation may allow to interpret laminated wedge structures as palaeoenvironmental archives. The identification of wedge-forming processes in (hyper-)arid environments implies that similar processes might also contribute to the formation of extra-terrestrial geomorphological features, such as on Mars. Amundson (2018) concluded that weathered soil from the surface of the Meridiani Planum on Mars is similar to the chemistry and morphology of hyperarid soils on Earth. Hence, the comparison of (hyper-)arid polygonal patterned soils with extra-terrestrial counterparts bears the potential to provide important insights for future Mars exploration.

The present study aims at resolving the processes and mechanisms governing wedge formation in a hyperarid setting, using calcium sulphate wedges formed in coarse-grained deposits of the Aroma alluvial fan situated on the Andean foreslope as study subjects. We propose different formation scenarios of wedge and surface crust development resulting from local haloturbation processes based on geochemical, mineralogical, sedimentological and microscopic investigations. Here we distinguish the Aroma wedge structures from wedge-polygon-formation processes evident in other parts of the Atacama Desert, e.g. thermal contraction mechanisms in the Yungay region (Sager et al. 2021), or desiccation polygon structures in playa-like environments (e.g. Ericksen 1981,1983; Bobst et al., 2001; Finstad et al., 2016).

2 Regional setting

The study site is located on the western Andean foreslope, north of the Quebrada Aroma (19° 39’ 34.02’’S, 69° 35’ 51.4’’W; Fig. 1A, B). On a regional scale, the western Andean foreslope is bordered by the rising Western Cordillera to the east and by the Central Depression and Coastal Cordillera to the west (Fig. 1A). Climatic conditions in the study area are characterised as hyperarid with a mean annual precipitation of <2 mm yr^{-1} (see isohyets in Fig. 1A; Houston, 2006). The Aroma fan and adjacent alluvial fans consist of alluvial gravels affiliated to the Upper El Diablo Formation of middle to late Miocene age (Muñoz and Sepúlveda, 1992; Farías et al., 2005; von Rotz et al., 2005; Evenstar et al., 2009; Hartley and Evenstar, 2010; Lehmann, 2013; Cosentino and Jordan, 2017), covered by gypsic relict soils and gypsisols (Cosentino and Jordan, 2017). In the vicinity of the study area, the Aroma fan surface has a mean slope of about 1.5° (Evenstar et al., 2009). At an altitude of ~1630 m a.s.l., we found a ~20–30 m long trench located adjacent to the A-457 road which had been excavated presumably during road construction works prior to 2017. The excavation exposed a network of subsurface soil cracks, which are up to ~2 m deep, and vertically laminated wedges developed within the alluvium of the Upper El Diablo Formation (Fig. 1C, D, E, G). Shattered cobbles and boulders (parent material) infiltrated by anhydrite and embedded in a

https://doi.org/10.5194/egusphere-2024-592
Preprint. Discussion started: 15 April 2024
© Author(s) 2024. CC BY 4.0 License.

calcium sulphate-rich matrix appear in the host sediment between the wedge structures (Fig 1H, I). The wedge network is covered by a ~20 cm thick surface crust dominated by calcium sulphate (Fig. 1E, F) which does not appear to form a polygonal patterned ground at its surface (Fig. 1B.1).

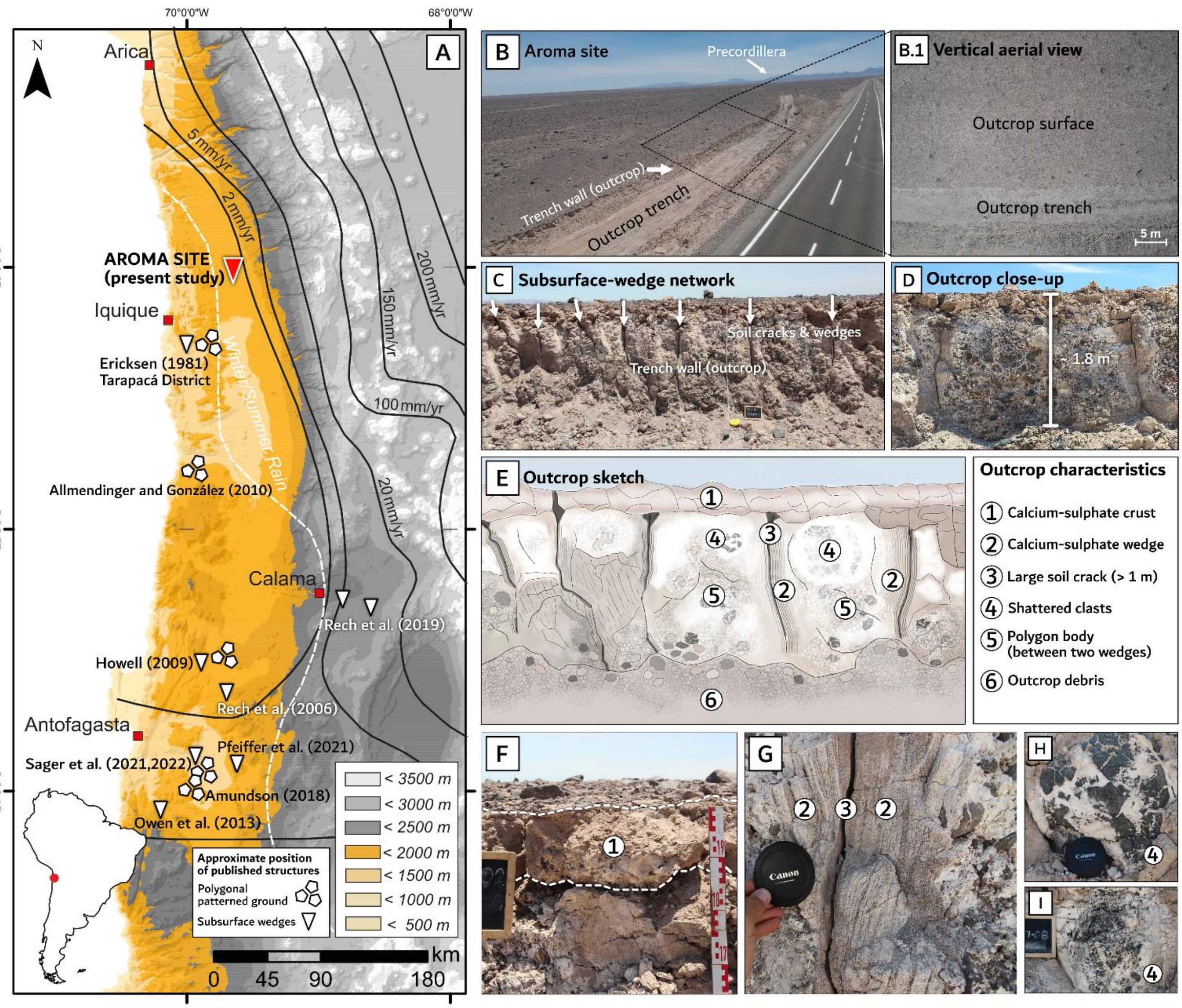

Figure 1: A) Colour shaded digital elevation model (derived from SRTM-data, created using ArcMap ver. 10.5.1) of northern Chile including isohyets (modified from Houston, 2006) as well as winter-rain and summer-rain dominated areas (white dashed line) after Houston (2006). The red inverted triangle indicates the study site situated on the Aroma fan. White inverted triangles and white polygons display published studies which investigated subsurface wedge structures and surface polygonal patterned grounds in the Atacama Desert. B) Oblique drone image of the Aroma outcrop viewing in NE direction. B.1) Nadir view of the outcrop surface showing no indications of polygonal patterned ground or similar surface expression. C) Outcrop trench wall (viewing in NW direction) displaying a subsurface network of large soil cracks (>1 m depth) and vertically laminated wedge structures. D) Close-up of

https://doi.org/10.5194/egusphere-2024-592
Preprint. Discussion started: 15 April 2024
© Author(s) 2024. CC BY 4.0 License.

outcrop structures and scale (viewing in NW direction). E) Outcrop sketch highlighting all important characteristics of the outcrop trench wall. Detailed description of the wedge network is given in the result section. F) Close-up photograph of the ~20 cm thick surface crust. G) Close-up photograph of subsurface crack and subsurface wedge parts to the left and to the right side of a soil crack. H) Shattered clast damaged by calcium sulphate intrusion. I) Shattered clast with a higher degree of destruction as in photograph H.

3 Material and methods

Sampling was conducted during two field campaigns in September 2017 and October 2018; all samples were collected from the north western trench sidewall. The sample set consists of six surface quartz clasts of pebble to cobble size sampled for surface exposure dating (see Fig. 2), a surface crust block containing various vertical and horizontal cracks, subsurface wedge parts, and shattered clasts from the host deposits (unconsolidated alluvium of the Upper El Diablo Formation). Figure 3 shows a schematic profile of the surface crust and the outcrop subsurface and its main sedimentological characteristics. All soil samples were thoroughly wrapped in foil after sampling to avoid subsequent contamination. We applied a multi-methodological approach to identify different mineral phases, (micro-)structures, and sedimentological characteristics of wedge and crust samples.

3.1 Geochemical, mineralogical, and sedimentological analyses

All mineralogical, geochemical, and sedimentological analyses of calcium sulphate wedge and crust subsamples were performed at the Institute of Geology and Mineralogy, University of Cologne, Germany. Since the extraction of individual very fine wedge laminae did not provide enough material for the analyses, small wedge parts (sets of laminae) were sampled along the horizontal axis of the wedge ARO18-08 from the wedge centre to the periphery. Figure 4 shows the sample ARO18-08 representing a horizontal cross section, or transect, of the wedge spanning between the periphery and centre of the wedge. The sample was fractured during sampling and hence consists of a left part (bordering the wedge periphery, hereafter abbreviated LP), and a right part (bordering the wedge centre, RP). Subsamples of the crust sample ARO18-02 were taken from the crust top surface downwards to the base of the crust (see Fig. 5).

The mineralogical composition of samples was determined by powder X-ray diffraction (XRD) analyses using a Bruker D8 AXS DISCOVER diffractometer with CuKα radiation (λ = 1.54058 Å) operating at room temperature. The patterns were collected between 7 and 120° 2θ with a step size of 0.010° 2θ and a dwell time of 1 s. All samples were refined by a whole powder pattern fitting using the Diffrac.TOPAS (Version 4.2) program with a Pearson VII function for profile fitting.

Prior to subsampling wedge sample ARO17-03A was used for high-resolution XRF scanning and radiographic imagery to resolve the fine vertical lamination (see Fig. 4). The wedge ARO17-03A was scanned with an ITRAX core scanner from CoxAnalytical Systems (Croudace et al., 2006) equipped with a Cr-tube using a scan resolution of 200 μm, a voltage of 30 kV and a current of 155 mA with an exposure time of 20 seconds.

https://doi.org/10.5194/egusphere-2024-592
Preprint. Discussion started: 15 April 2024
© Author(s) 2024. CC BY 4.0 License.

Scanning electron microscopy (SEM) was performed on wedge ARO18-08 (2x LP, 1x RP) and crust sample ARO18-02 to analyse microstructures and calcium sulphate cement using a Zeiss Sigma 300-VP equipped with an electron dispersive X-ray spectroscopy (EDX). Prior to the SEM and EDX analysis, the samples were cut, embedded in an epoxy-resin puck of 2.5 cm in diameter, and subsequently gold-sputtered (see sample puck examples in Fig. S.10 in the supplementary material).

Grain-size analysis was conducted using a laser particle analyser from Beckman Coulter LS13320. Prior to sample preparation, the calcium sulphate cement was removed from the bulk sample of wedge ARO18-08 and surface crust ARO18-02 by dissolving the samples in 10 % NaCl solution for 7–10 days. The clastic material of the samples was subsequently treated with 5 % H_2O_2 to remove any potential organic content and was subsequently etched with 10 % HCl to remove carbonate before the sample was dispersed in a 2.5 % sodium polyphosphate solution.

ICP-OES analysis was performed using an ARCOS ICP-OES with an axial plasma observation from SPECTRO Analytical Instruments. Sample water extraction of subsurface wedges ARO17-03A and ARO18-08 as well as surface crust sample ARO18-02 followed the procedure detailed by Voigt et al. (2020) to analyse the concentration of soluble salts besides calcium sulphate within the sediment material. Concentrations of Ca and S were not considered for analysis as calcium sulphate phases were dissolved to saturation levels in the leachates.

Photogrammetric 3D reconstructions of subsurface wedge (ARO17-03A) and surface crust (ARO18-02) samples were created from image datasets taken in a lightbox environment with a fixed physical camera position and a turntable (see Table S.7 and further information in supplementary material for more details). Final watertight and scaled meshes (~10 M faces) were used to quantify the specimens' volumes and to determine the bulk density of the samples.

3.2 Dating methods

Surface exposure dating was conducted following the noble gas extraction procedure of Ritter et al. (2021) to measure the concentration of cosmogenic ^{21}Ne in six surface quartz clasts (ARO17-01A–F) from the Aroma fan surface above the studied wedge network (see Fig. 2). During the sampling process in the field, we took care to avoid sampling clast fragments sourced from 'Kernsprung' (insolation weathering) and sampled in an area of approx. 40–50 m^2. Samples were crushed, sieved to 250–710 µm, and etched multiple times in HCl and a HF-HNO_3 mixture (Kohl and Nishiizumi, 1992). The ^{21}Ne exposure ages shown in Figure 2 (relative probability plot) are based on the LSD$_n$ scaling scheme of Lifton et al. (2014) and calculated with the CRONUS-Earth online calculators (version 3; https://hess.ess.washington.edu/math/v3/v3_age_in.html) as published by Balco et al. (2008). Cosmogenic nuclide and calculation data as well as ^{21}Ne triple isotope diagram for the respective exposure ages are provided in the supplementary material (Fig. S.4 and S.5; Data tables: Table S.1 and S.2).

https://doi.org/10.5194/egusphere-2024-592
Preprint. Discussion started: 15 April 2024
© Author(s) 2024. CC BY 4.0 License.

^{239}Pu analysis was performed to trace any recent (i.e., Anthropocene) transport of surface sediment into the subsurface through the surface crust. Plutonium subsamples were collected from the calcium sulphate crust ARO18-02 (see Fig. 5). First, we sampled the dust covering the top surface of the crust using a clean brush (ARO18-02-001 and replicate sample ARO18-02-TC2). Afterwards, we sampled a cavity located ~10 cm below the top surface of the crust (ARO18-02/Pu5) using a long spatula and a vacuum grain picker with a mounted cannula tip. Note that the sample ARO18-02/Pu5 was taken from a different location than indicated in Figure 4 (see Fig. S.9 in the supplementary material for the exact subsample position). The cavity was not exposed at the outcrop, minimising the possibility of pre-sampling contamination due to the road construction works. To avoid sampling of potentially contaminating dust particles (e.g., particles blown in during sample transport), we sampled surfaces located deeply inside the cavity (>4–5 cm behind the cavity opening). Afterwards, we cleared a vertical profile along one side of the crust block by removing ~1–3 cm of the outer surfaces (see Fig. S.8 in the supplementary material) using a handheld rotary tool with a steel blade mounted. Along this profile, we sampled three blocks of 1.5 cm thickness each along the profile (ARO18-02/Pu2: 0–1.5 cm below the horizontal top surface; ARO18-02/Pu3: 1.5-3.0 cm; ARO18-02/Pu4: 3.0–4.5 cm) to investigate downward migration of dust particles inside the heterogenous dense crust. The fragility of the crust block material required a top-down sampling strategy, introducing a certain risk of contamination of the deeper sample with material falling down from above. We mitigated that risk by constantly vacuum-cleaning the surfaces and narrowing the horizontal cutting area at depth. After chemical processing (see supplementary text for details), the samples were measured at CologneAMS (Dewald et al. 2013). Measuring ^{239}Pu using accelerator mass spectrometry (AMS) bears the advantage of high measurement accuracies achievable for small quantities of sample material (for a comprehensive overview see e.g. Alewell et al., 2017). We further attempted to quantify ^{240}Pu from the same sampling material, but an unusual piling of counts at the targeted mass per charge ratio caused most measurements to be unreliable (exception: ARO18-02-TC2).

4 Results

4.1 Calcium sulphate wedge analyses

The investigated outcrop extends to a depth of ~1.8–2 m. Below the surface crust are coarse-grained, calcium sulphate-cemented sediments comprising clasts ranging in size from pebbles to boulders (‘polygon body’; see Fig. 3c). Many clasts are shattered and cracks are filled with calcium sulphate (see S.3 in the supplementary material). The polygon bodies comprise a network of large soil cracks (vertical extent >1 m, see Fig. 3b, c) and adjacent, vertically laminated parts left and right of the crack, which represent the calcium sulphate wedges. The base of the trench outcrop is covered by debris. ^{21}Ne surface exposure ages of the surface clasts vary from 3.3 ±

https://doi.org/10.5194/egusphere-2024-592
Preprint. Discussion started: 15 April 2024
© Author(s) 2024. CC BY 4.0 License.

0.3 to 5.4 ± 0.4 Ma with a mean age of 4.34 ± 0.36 Ma (further detailed information in the supplementary material).

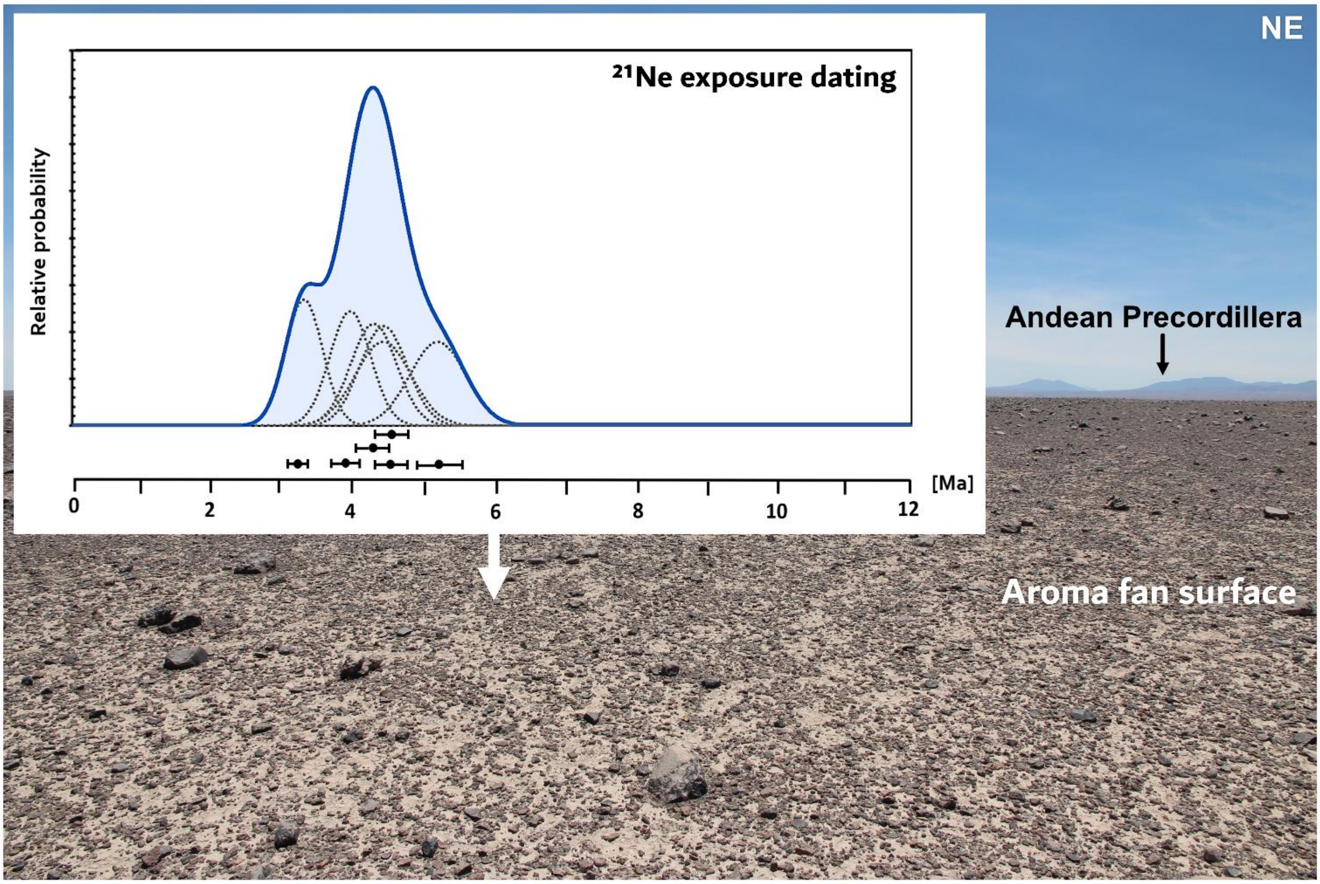

240 **Figure 2: Aroma fan surface viewing in NE direction and relative probability functions of individual surface quartz clasts (ARO17-01A–F; grey dotted) and cumulative curve (blue shaded). Error bars (±1σ) are based on the external errors (see Table S.2 in the supplementary material). The cumulative curve indicates a distinct peak at ~4.3 Ma.**

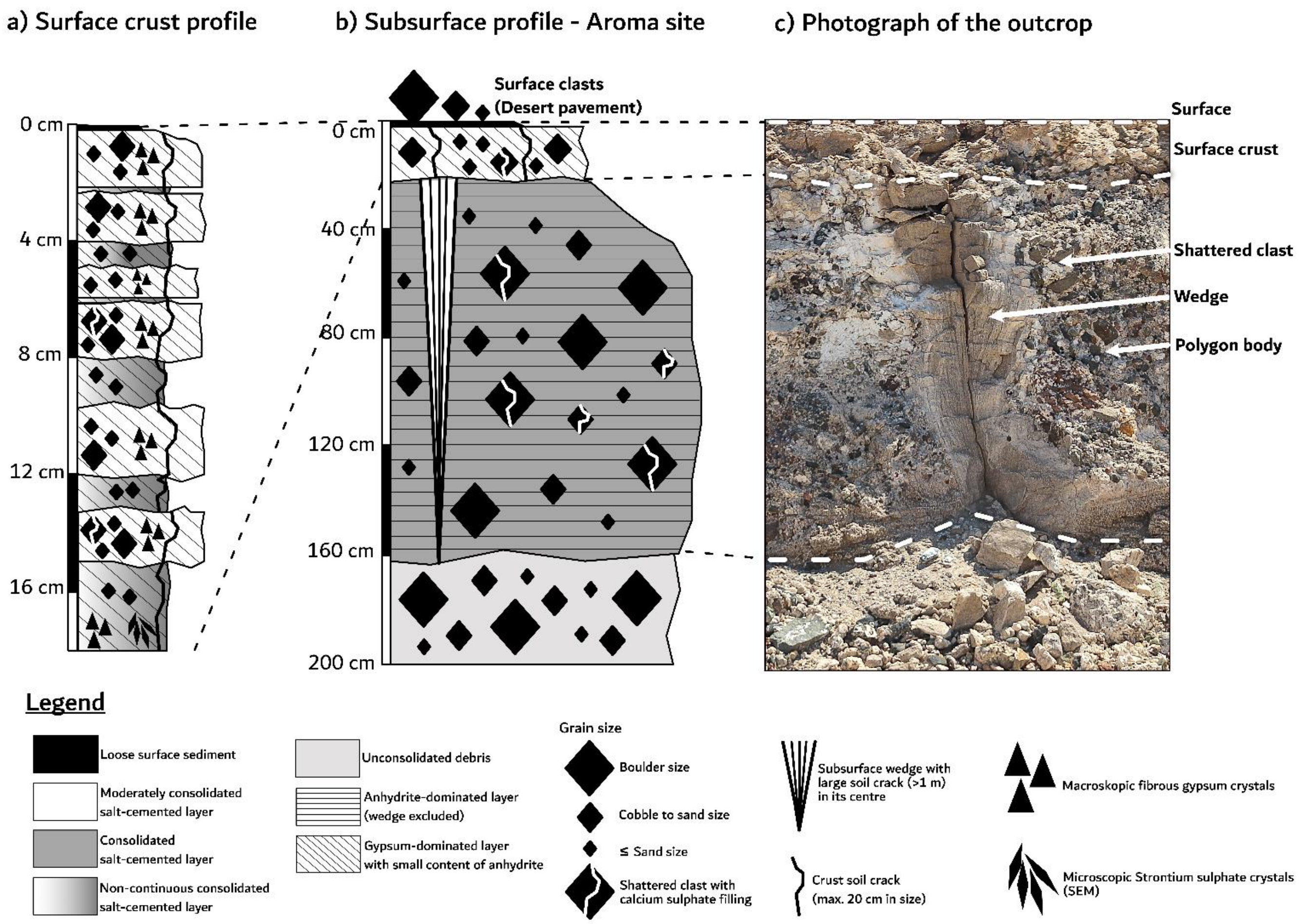

Figure 3: a) Schematic profile of the ~20 cm thick surface crust showing its main sedimentological characteristics. The surface crust is characterised by moderately consolidated layers exhibiting macro-crystalline gypsum crystals, which are interrupted by non-continuous consolidated layers ("lens-like") consisting of microcrystalline gypsum-dominated cement. The crust shows large horizontal and vertical cracks (up to ~20 cm) partly containing loose cobbles. SEM analysis revealed microscopic lenticular $SrSO_4$ crystals only in the base layer of the crust. b) Schematic subsurface profile of the outcrop depicting main characteristics; desert pavement, surface calcium sulphate crust, calcium sulphate-cemented matrix with incorporated pebble to boulder sized clasts (representing the 'polygon body') containing a network of vertical cracks and vertically laminated calcium sulphate wedges. Shattered clasts with calcium sulphate fillings occur within the polygon body. c) Photograph of the outcrop.

XRD results of salt precipitates from two shattered clast samples (ARO18-04 and ARO18-05) revealed ~70 wt% of β-anhydrite, ~20–30 wt% of other evaporites, and ~0.5–15 wt% clastic material in the cement matrix (see Fig. S.3 in the supplementary material). The group of other evaporites comprises up to 17–30 wt% aluminite ($Al_2SO_4(OH)_4{\bullet}7H_2O$), and traces of konyaite ($Na_2Mg(SO_4)_2{\bullet}5H_2O$) and halite (see Table S.4 in the supplementary material).

The vertical lamination of the calcium sulphate wedges (Fig. 4; laminated part) extends from the centre of the wedge (soil crack in the outcrop) to the periphery (polygon body direction). Lamination of the wedges is less

https://doi.org/10.5194/egusphere-2024-592
Preprint. Discussion started: 15 April 2024
© Author(s) 2024. CC BY 4.0 License.

distinct at the periphery (see Fig. 4B and 4C; radiographic image). Wedge sample ARO17-03A was used to calculate the bulk density from the photogrammetrically derived 3D model, yielding a density of 1.68 ± 0.04 g/cm^3 (see supplementary material for more details).

The (evaporite-free) clastic sediments in wedge ARO18-08 are dominated by sand, with medium and fine sand being the most abundant grain sizes. SEM images taken at three different positions along the wedge transect reveal different densities of calcium sulphate cementation, with the general pattern of increasing densities towards the periphery and decreasing densities towards the centre of the wedge. The SEM images taken from the centre of the wedge (RP) and close to the periphery (LP) show that the cementation density varies randomly within the wedge depending on the cement content of the individual fine laminae. The generally high content of calcium sulphate cement varies between ~40–70 wt% and the clastic content varies between ~26–50 wt% at the periphery and ~50–60 wt% at the centre of the wedge (see Fig. 4 B.2; XRD results). The Ca and S compositions in wedge ARO17-03A (Fig. 4C) match, and increase towards the periphery, in particular within the non-laminated part of the wedge. The XRD results of wedge ARO18-08 indicate that gypsum is mainly distributed in the RP, reaching the highest gypsum content in subsample 1 and 2 at the wedge centre with ~40 wt% gypsum. The dominant calcium sulphate phase of the wedge is anhydrite with up to ~73 wt% in the LP, decreasing to a minimum abundance (~3 wt%) in RP close to the wedge centre (see Table S.4 in the supplementary material). The Na and Cl concentrations based on ICP-OES results show that Na and Cl were both dissolved in the leachates during the sample water extraction procedure (see Table S.3 in the supplementary material). The increased Na concentration indicates that halite but also other sodium- and chloride-bearing soluble salts could be present in the samples, but are not resolvable in our ICP-OES data. However, the XRD results of some wedge subsamples show traces of other sulphates occurring besides calcium sulphate such as aluminite, arcanite (K_2SO_4), amarantite ($FeSO_4(OH)\cdot 3H2O$), and peretaite ($Ca(SbO)_4(SO_4)_2(OH)_2$) (see Table S.4 in the supplementary material).

https://doi.org/10.5194/egusphere-2024-592
Preprint. Discussion started: 15 April 2024
© Author(s) 2024. CC BY 4.0 License.

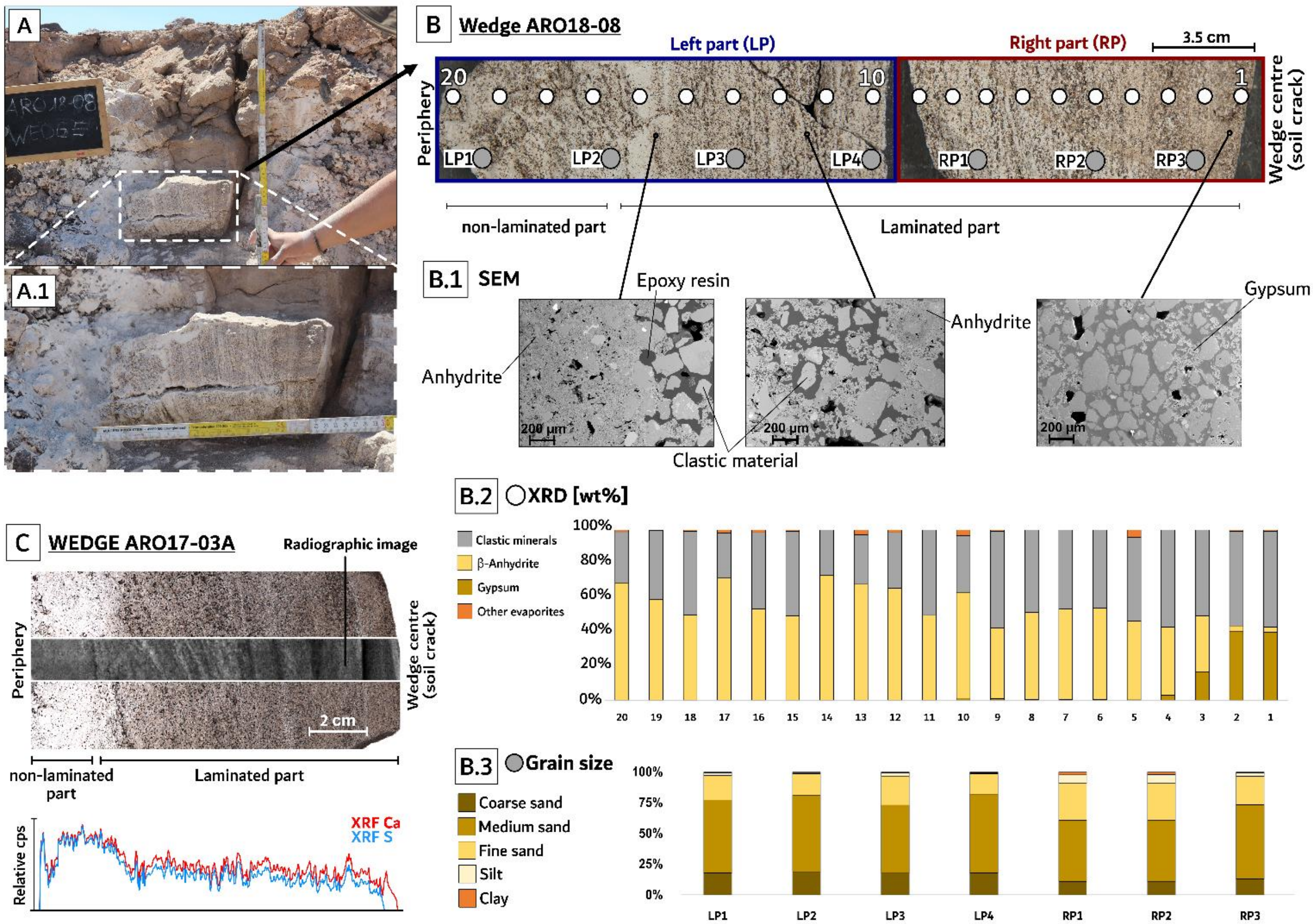

Figure 4: A) Outcrop image and close-up (A.1) of wedge ARO18-08 sampled from the outcrop wall at ~40–50 cm depth. B) Photograph of vertically laminated wedge ARO18-02 showing laminated and non-laminated sections and the outcrop orientation of the wedge (right: wedge centre; left: periphery). The positions of the XRD and ICP-OES subsamples (see Tab. S.3 in the supplementary material for ICP-OES results) are indicated by white circles and the subsamples for grain size analysis are indicated by grey circles. B.1) SEM images of three positions within the wedge sample showing different densities of calcium sulphate cementation. B.2) XRD results of 20 wedge subsamples (white circles). B.3) Grain size results of wedge subsamples (grey circles). C) Photograph and radiographic image of wedge ARO17-03A. The XRF results show a correlation between Ca and S throughout the wedge. The very fine lamination is also visible in the fluctuations of the XRF Ca and S contents.

4.2 Surface crust analyses

The surface crust represents the top ~12–20 cm of the studied outcrop (see Fig. 3 and Fig. S.7 in the supplementary material). The crust top surface is covered by dust and a large quantity of clastic material larger than sand, typical for an unconsolidated desert pavement (see Fig. 2 and Fig. S.2 in the supplementary material). Below the surface, the crust is moderately cemented, predominantly by gypsum. The bulk density derived from

https://doi.org/10.5194/egusphere-2024-592
Preprint. Discussion started: 15 April 2024
© Author(s) 2024. CC BY 4.0 License.

the photogrammetric 3D model of the sample block ARO18-02 is 1.34 ± 0.03 g/cm^3 (see supplementary datasets for more details).

Grain size data from clastic material of four crust subsamples indicate a dominance of the medium to fine sand fraction across the crust (Fig. 5). Microscopic images show fibrous macrocrystalline gypsum crystals on consolidated wavy and partly 'nodule-like' microcrystalline calcium sulphate cement (Fig. 5). The crust surface contains ~43 wt% clastic minerals, ~35 wt% of aluminite ($Al_2SO_4(OH)_4{\bullet}7H_2O$), and traces of gypsum (~0.8 wt%) as revealed by the XRD measurements. Subsamples taken from a few centimetres below the surface (ARO18-02-002 and all samples below) show a considerable change in mineralogy as the gypsum content increases up to ~70–90 wt % while the clastic mineral content decreases to <11 wt% with increasing depth. The β-anhydrite content increases with increasing depth from ~1 wt% in the upper part to up to ~24 wt% in the bottom crust sample ARO18-02-007. The Na and Cl concentrations based on ICP-OES results are below the detection limit for all crust subsamples except for the bottom sample ARO18-02-007 (0.77 mol/l Na), indicating a general absence of NaCl in the surface crust. The presence of other sulphates is confirmed by XRD results, which indicate the presence of aluminite, alunogen ($Al_2(SO_4)_3{\bullet}17H_2O$), konyaite, and ramsbeckite ($(Cu,Zn)_{15}(SO_4)_4(OH)_{22}{\bullet}6H_2O$). Subsample ARO18-02-007 shows microcrystalline lenticular crystals of celestine ($SrSO_4$) as illustrated by the SEM and EDX element distribution images (Fig. 5; SEM3).

The crust is characterised by a generally high porosity and large cracks (>15 cm in size) containing gypsum crystals and pebble to cobble-sized clasts (see crust photo in Fig. 5). The highest blank-corrected ^{239}Pu concentrations were measured on the crust surface (Fig. 5; ARO18-02-001, 6.48 ± 0.20 mBq kg^{-1}, ARO18-02-TC2, 6.09 ± 0.23 mBq kg^{-1}) and in the sampled cavity (ARO18-02/Pu5; 8.68 ± 0.59 mBq kg^{-1}). These values are well in range of what has been measured close to the city of Iquique at similar latitudes (~20°S, ~7 mBq kg^{-1} assuming a soil density of 1.8 g cm^{-3} and an isotope ratio of ~0.17; Chamizo et al., 2011). Due to low count rates, blank correction amounted to >20 % for ^{239}Pu measurements of subsamples ARO18-02/Pu2, ARO18-02/Pu3 and ARO18-02/Pu4 (see Table S.5 in the supplementary material). We consider these blank subtraction values as being too high to draw any detailed conclusions from the individual blank-corrected concentrations. However, the low count rates reflect extremely low nuclide concentrations (blank-corrected concentrations <1.19 ± 0.15 mBq kg^{-1}) in these subsamples. We report a similar blank subtraction of 22% for the ^{240}Pu measurement of ARO18-02-TC2, which is related to high blank levels. While similar constrains on the blank-corrected ^{240}Pu concentration of this sample apply as valid for the other subsamples with high relative measurement background levels, it is worth to note that the resulting ^{240}Pu/^{239}Pu is 0.185 ± 0.020. This ratio reflects the global fallout signature, i.e. the source of the plutonium measured in the samples is likely to be originating from the atmospheric weapon tests conducted during the 1950s and 1960s (i.e. ^{240}Pu/^{239}Pu = 0.173 ± 0.027 for 0-30°S; Kelley et al., 1999; 0.166 ± 0.008 for Iquique at ~20°S, Chamizo et al., 2011).

https://doi.org/10.5194/egusphere-2024-592
Preprint. Discussion started: 15 April 2024
© Author(s) 2024. CC BY 4.0 License.

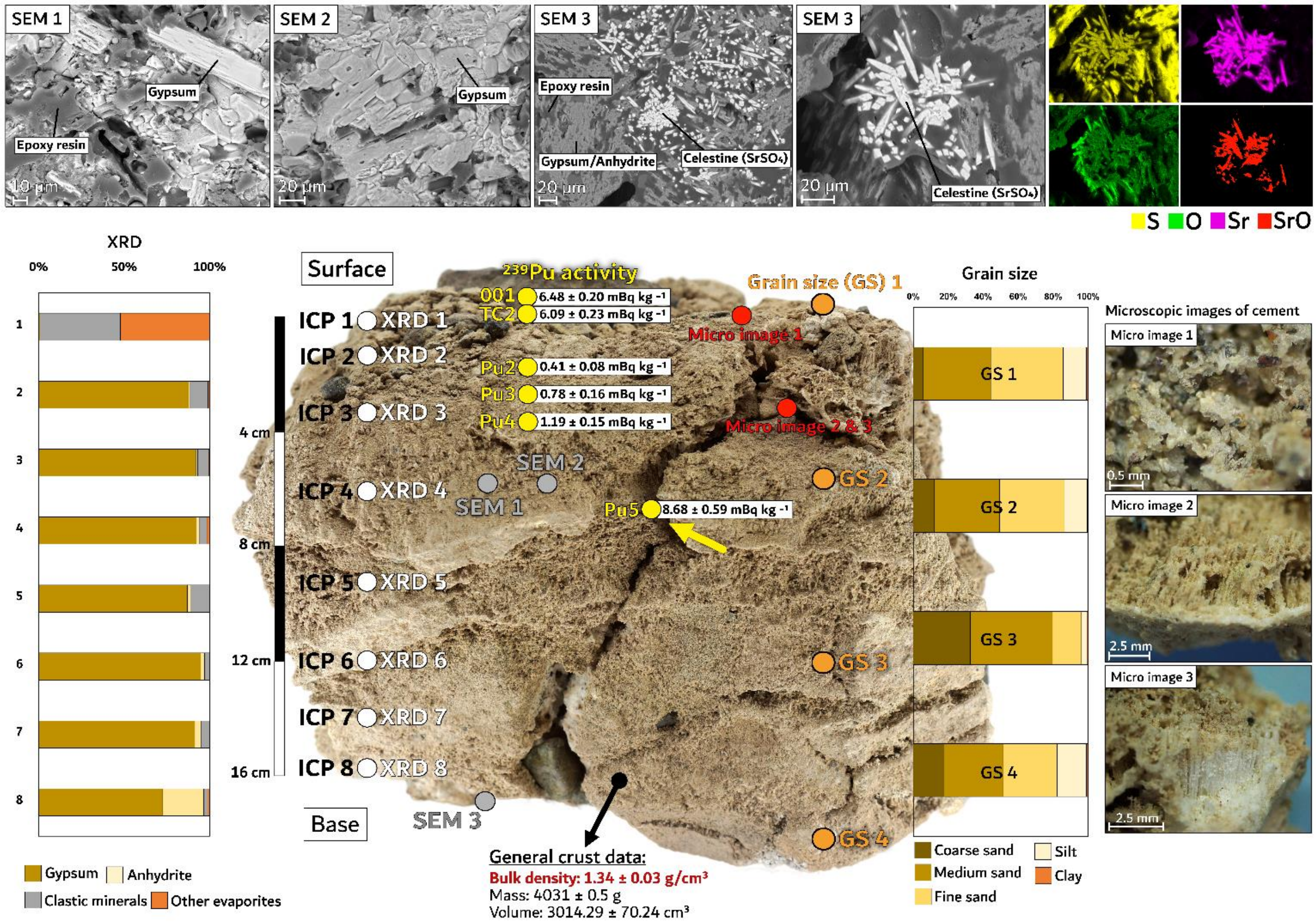

Figure 5: Photograph of ARO18-02 (surface crust) and compilation of applied analyses. The surface crust is characterised by a high clastic mineral and evaporite content (except for calcium sulphate) on the surface and a generally high gypsum content in the subsamples below the surface (see XRD results; white circles). The clastic sediment is dominated by medium to fine sand (see GS subsamples; orange circles). The cement includes fibrous and microcrystalline gypsum crystals (see micro images 1–3; red circles and SEM1 and 2; grey circles). SEM3 shows lenticular crystals of celestine ($SrSO_4$), which occurs only in crust base subsample ARO18-02-007. The highest ^{239}Pu activities (yellow circles) are in the surface and crack interior subsamples.

5 Discussion

5.1 Formation hypothesis of subsurface wedges and polygonal patterned ground

The high content of calcium sulphate in the investigated subsurface wedges contrasts with previous descriptions of wedge-polygon-structures in the Atacama Desert and could imply that calcium sulphate-driven haloturbation processes dominate wedge-polygon-formation at the Aroma fan site rather than thermal contraction (low-salt

https://doi.org/10.5194/egusphere-2024-592
Preprint. Discussion started: 15 April 2024
© Author(s) 2024. CC BY 4.0 License.

sand wedges; Sager et al., 2021) or polygon formation in playa-like environments due to desiccation (e.g. Ericksen 1981,1983; Bobst et al., 2001; Finstad et al., 2016).

Previous studies suggested that dissolution and precipitation of salts are the most important processes contributing to salt heave processes in the Atacama Desert (Buck et al., 2006; Howell, 2009) and clast shattering (Winkler and Singer 1972; Amit et al., 1993; Rodriguez-Navarro and Doehne, 1999), as the solution supersaturation ratio is proportional to the crystallisation pressure (Winkler and Singer, 1972), a pattern that is controlled by high evaporation rates and solute availability (Howell, 2009). The dissolution and precipitation processes of calcium sulphate are evident from the high content of the naturally occurring β-anhydrite in the wedge and in the shattered clasts from the Aroma fan outcrop (Fig. 1). The β-anhydrite is thought to be formed exclusively by the precipitation from a highly saline solution at temperatures as low as 60°C (Hardie, 1967; Cody and Hull, 1980). However, the formation under ambient desert conditions is still a matter of debate (Ritterbach and Becker, 2020; Wehmann et al., 2023). The gypsum content in the wedge samples cannot yet be identified as primary or secondary gypsum. The latter is formed by the rehydration of γ-anhydrite over bassanite back to gypsum (Mossop and Shearman, 1973) and would imply that swelling and shrinking processes contribute to haloturbation mechanisms in the subsurface. Shi et al. (2022) proposed that tunnels in the hexagonal crystal structure of γ-anhydrite from the Atacama Desert can incorporate cations of silicon and phosphorous, which are thought to attenuate phase transition from γ-anhydrite to bassanite. The authors discussed that this phenomenon enables γ-anhydrite to be prevalent in hyperarid environments such as the Atacama Desert and Mars. Ritterbach and Becker (2020) concluded that the dehydration of gypsum to bassanite and further to β-anhydrite may require long periods of time at temperatures of 80 °C and even lower, which may explain the presence of β-anhydrite in deposits from hyperarid environments.

The hyperarid soil genesis model of Howell (2009) may be applied to understand wedge formation mechanisms in our study area (Fig. 6). Based on this model, a sequence of wedge formation could begin with the supply of meteoric water from a moisture event, followed by infiltration into the coarse-grained and poorly sorted alluvium of the Aroma fan site. During infiltration, the meteoric water is assumed to dissolve soluble salts and hence to carry the downward migration of these salts (see Fig. 6, step 1). At greater depths, the saline solution exceeds saturation and salts precipitate in the pore space of the alluvium (Fig. 6, step 2). The resulting destructive crystallisation pressure of the precipitated salts causes significant mechanic damage in the surrounding deposits as reported in previous studies (e.g. Buck et al., 2006; Howell, 2009; Benavente et al., 2006; Schiro, et al., 2012; Flatt et al., 2014). Fracturing processes in the Aroma fan outcrop are reflected by numerous soil cracks in the deposits as well as by shattering in clasts from cobble to boulder size (see Fig. 1 and S.1, S.3 in the supplementary material). Stress caused by subsurface volume increase in the polygon body leads to a preferred deformation along the axis of least resistance, i.e. upwards, and is referred to as salt heave processes (Buck et al. 2006).

https://doi.org/10.5194/egusphere-2024-592
Preprint. Discussion started: 15 April 2024
© Author(s) 2024. CC BY 4.0 License.

The surface sediment is deposited in soil cracks formed by subsurface pressure. A specific sediment transport mechanism cannot be determined as the well-sorted grain size distribution of the wedge material (mainly medium to fine sand fraction, Fig. 4) indicate aeolian deposition, but due to the potential for intermittent rainfall events at the Aroma fan site, low-magnitude fluvial transport (confined to the debris on top of the wedge) cannot be excluded.

Repeated cycles of frequent moisture events, or intermittent phases thereof, may have caused the accumulation of salts within the soil crack. Swelling and shrinking processes due to the phase transformation of gypsum to γ-$CaSO_4$ and vice versa could have led to an increase in crack width and depth, as well as increased clast fracturing (see Fig. 6, step 3; cf. Howell, 2009). As a result, surface sediment, salts and moisture can rapidly infiltrate to greater depths, and enlarged soil cracks act as 'salt and moisture conduits', allowing haloturbation to occur in even deeper deposits (Howell, 2009).

Salt heave processes intensify as moisture events and haloturbation processes are repeated over time, gradually forming a microtopographic signature that represents a polygonal patterned ground on the surface (see Fig. 6, step 3; cf. Buck et al. 2006; Howell, 2009). Note that the purple dashed lines in step 6 (Fig. 6) only show a hypothetical polygonal patterned ground beneath the surface crust, as there is no evidence of a microtopographic signature at the base of the surface crust sample. Repeated haloturbation (shrinking and swelling) leads to tensile stresses in the cohesive material and develops expansion and contraction forces, resulting in reopening of cracks that are refilled during the next depositional cycle (Howell, 2009). This mechanism has probably caused the formation of a vertical lamination of the Aroma fan wedges, consisting of calcium sulphate and clastic-dominated sediment (cf. Howell, 2009). Apart from visual interpretation, the lamination is evident from the XRD and XRF results of both wedges, as well as the radiographic image of wedge ARO17-03A (Fig. 4, 6.4, 6.5). As shown in Figure 3B and 3C, both analysed wedges show a non-laminated and β-anhydrite-dominated part at the wedge periphery, the origin of which is not clear yet. This part could either represent the stratigraphically oldest part or initial wedge growth phase prior to or simultaneously with the initial crack opening, or it could indicate that the layer set close to the periphery and the polygon body material was homogenised during intensified haloturbation stresses in the subsurface. The dominance of β-anhydrite is presumably caused either by direct precipitation from highly saline solutions or by dehydration of gypsum to bassanite on to β-anhydrite, provided that the phase transition occurs over a long period of time (Ritterbach and Becker, 2020). The increased gypsum content in the subsamples ARO18-08-RP1–4 directly at the wedge centre (soil crack side) indicates a phase transition from gypsum to anhydrite. This process is associated with a volume decrease of ~29 % for the gypsum-bassanite transition (Milsch et al., 2011) and a total of ~39 % for the gypsum-anhydrite transition (Milsch et al. 2011; Sanzeni et al. 2016). Such volumetric changes could result in ‘shrinking stress’ leading to reopening of the soil crack. Thus, we interpret that shrinking processes dominate in the wedge centre, causing repeated

https://doi.org/10.5194/egusphere-2024-592
Preprint. Discussion started: 15 April 2024
© Author(s) 2024. CC BY 4.0 License.

reopening of the soil crack, rather than dissolution precipitation of calcium sulphate, which dominates in the polygon body, causing salt heave.

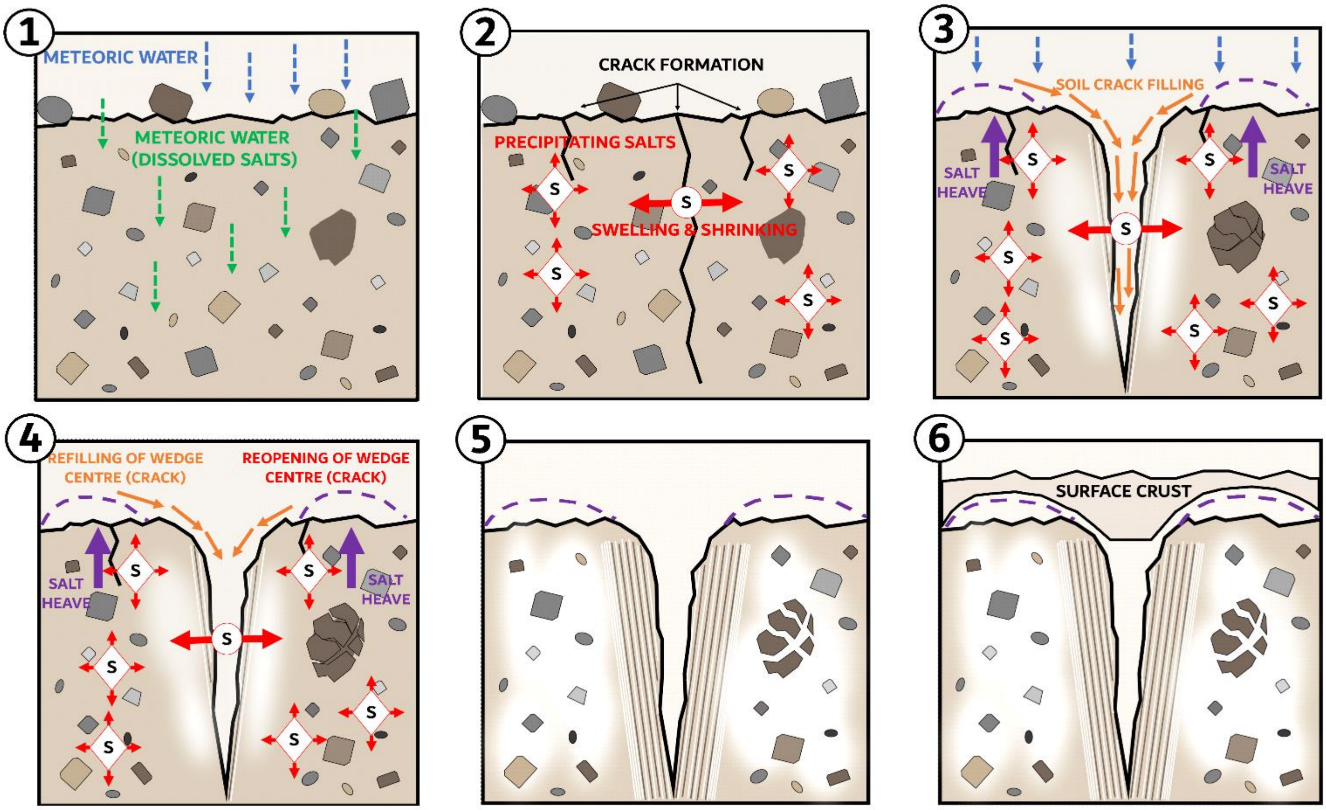

Figure 6: Sequence of wedge formation processes in the subsurface of the Aroma fan site base on the hyperarid soil genesis model of Howell (2009). 1) Meteoric water infiltrates porous alluvium and dissolves soluble salts, which precipitate in the pore space and indurate the alluvial sediment. 2) Haloturbation (e.g. swelling/shrinking and dissolution/precipitation of calcium sulphate and other salts) creates a destructive pressure in the subsurface, leading to the formation of soil cracks and subsequent filling of the soil cracks with surface sediment. Significant subsurface pressure results in salt heave (Buck et al. 2006), where the subsurface pressure is released upwards, as this is the direction of least resistance (purple arrows). 3) Meteoric water re-infiltrates the alluvium and the processes of 1) and 2) are repeated, resulting in soil crack growth (both in width and depth) and clast shattering in the sediment. The haloturbation and subsequent reproduction of soil cracks promotes the infiltration of sediment, salts and moisture to greater depths. 4) Multiple cycles of haloturbation (dominated by swelling and shrinking due to dehydration of gypsum or hydration of γ-anhydrite) cause reopening and refilling of cracks. As a consequence, larger soil cracks can develop wedge structures to the left and to the right side of the crack 5) The product of long-term haloturbation processes in the subsurface associated with multiple moisture events is the characteristic vertical lamination of calcium sulphate wedges as well as a polygonal patterned ground (microtopographic signature, purple dashed lines) on the surface due to salt heave mechanisms. 6) Probably after wedge-polygon-formation, the surface crust covers the polygonal patterned ground, indicating an environmental change that favoured the formation of the crust. The purple dashed lines represent only a hypothetical polygonal patterned ground, as the surface crust sample shows no evidence of a microtopographic signature at its base.

https://doi.org/10.5194/egusphere-2024-592
Preprint. Discussion started: 15 April 2024
© Author(s) 2024. CC BY 4.0 License.

5.2 Formation hypothesis of the surface crust

Calcium sulphate-rich soils and surface crusts in the Atacama Desert are described in numerous previous studies (e.g. Rech et al., 2003; Ewing et al., 2006; Wiezchos et al. 2010; Wang et al., 2015; Rech et al., 2019; Ritter et al., 2022). These calcium sulphate-rich soils and crusts are formed by atmospheric deposition (Rech et al., 2003; Wang et al., 2015; Rech et al., 2019) and contribute significantly to landscape protection against erosion (e. g. Mohren et al., 2020a; Ritter et al., 2022), covering large areas of the Atacama Desert (e.g. Hartley and May, 1998; Ericksen 1981,1983; Rech et al., 2003; Ewing et al., 2006; Rech et al., 2006; Ritter et al., 2022).

The ^{21}Ne exposure ages (4.34 ± 0.36 Ma) of the desert pavement quartz clasts from the Aroma fan surface near the outcrop could imply that the pebbles and cobbles, remaining stationary after deposition, were lifted by blown-in accretionary dust ('born at the surface model'; Wells et al., 1995). Our ^{21}Ne surface exposure ages broadly fit the surface formation pulses at ~7 Ma and ~3 Ma, as described by Evenstar et al. (2009). It should be noted that these authors measured ^{3}He from ~0.5–1 m boulders (including samples taken in the vicinity of our sampling site) and used a different scaling scheme (the St scaling scheme; Lal 1991 and Stone 2000). Applying the latter, our surface exposure ages would cluster at ~5.4 Ma (see Table S.2 in the supplementary material). These age ranges indicate the end of alluvial deposition and the onset of significant accumulation of gypsum by atmospheric deposition at the transition from the Late Pliocene to the Early Pleistocene. Thus, despite the lack of absolute ages of the surface crust and the subsurface wedges, we suggest that the stratigraphically younger surface crust may have formed after the formation of the subsurface wedges. Since the subsurface wedge system has formed due to multiple moisture events (haloturbation processes), climatic conditions could have changed from marginally 'wetter' conditions to present-day hyperaridity. The presence of surface crust rather indicates a net accumulation of atmospheric dust during more drier conditions.

Considering the absence of polygonal patterned ground on the surface of the Aroma fan, we suggest that the surface crust covered the patterned ground and might have attenuated haloturbation processes in the subsurface, as arid conditions favoured the accumulation of gypsum rather than redistribution and secondary modification of gypsum deposits from the surface.

On modern timescales, our ^{239}Pu data indicate that sediment fines migrated along cracks towards the inner crust during the past ~70 years. We measure comparably high and consistent ^{239}Pu concentrations in the surface samples, while the dense crustal parts immediately below the crust top surface have ^{239}Pu concentrations at the detection limit. After deposition, plutonium isotopes adsorb to soil fines, and downward migration of ^{239}Pu can be governed by physical processes (for an overview on the environmental behaviour of Pu isotopes see e.g. Alewell et al., 2017). Consequently, low ^{239}Pu concentrations inside the dense parts of the crust could be expected, contrasting higher ^{239}Pu concentrations measured inside the crustal cavity. The apparent relocation of Pu-marked fines to ~10 cm depth during the past ~70 years implies that sediment (and likely moisture) transport to the

https://doi.org/10.5194/egusphere-2024-592
Preprint. Discussion started: 15 April 2024
© Author(s) 2024. CC BY 4.0 License.

subsurface is still an active process in recent times. Such a relocation of fines is likely to occur along inner-crust cracks. It remains unresolved whether fractions of surface sediments and/or moisture can transit the crust in its present-day state over the long-term to feed processes forming the wedge-polygon-system.

However, it appears that the wedge-polygon-system, subsurface haloturbation and salt heave forces have become significantly weakened since the crust formed. The absence of polygonal patterned ground on the Aroma fan surface might be due to inhibited salt heave processes, as haloturbation is still present but not as intense as prior to crust formation. The attenuated haloturbation forces in the subsurface could have at least led to stress in the surface crust, which developed numerous cracks enabling surface material migration into the subsurface.

5.3 Implications of the formation of other evaporites in the Aroma fan deposits

XRD measurements on samples taken from wedge ARO18-08 revealed traces of hydrated sulphate phases such as aluminite (and probably other Na- and Cl-bearing salts not distinguishable by ICP-OES results from ARO18-08). This finding may imply that multiple cycles of dissolution and precipitation may have caused salt dissolution and alteration of weathering-sensitive minerals such as feldspar, which is abundant in our sample material. Chukanov et al. (2013) first described the mineral vendidaite ($Al_2(SO_4)(OH)_3Cl{\cdot}6H_2O$) from a copper mine in the Antofagasta region, which is chemically similar to the hydrated aluminite present in the Aroma fan material. The occurrence of these 'exotic' aluminium-bearing salts is interpreted by Chukanov et al. (2013) as indicator for feldspar alteration, favoured by exposure to sulphuric acid resulting from oxidation of primary sulphates. Joeckel et al. (2011) also concluded that the presence of aluminite (among other Al-bearing sulphates) in the deposits may reflect long-term exposure of rocks or sediments to weathering in natural environments. Aluminite is also detected in the fractured clasts in the polygonal body of the Aroma fan outcrop (from ~110 cm depth below the surface) and makes up ~35 wt% of the surface sediment, as indicated by the XRD results of surface subsample ARO18-02-001 (see diffractogram in Fig. S.6 in the supplementary material). This finding suggests that feldspar alteration occurs at different depths (surface and subsurface) along the outcrop. In contrast to the copper-dominated study site of Chukanov et al. (2013), and considering the mineralogical composition of the Aroma fan samples, acidic weathering is unlikely to cause primary sulphate oxidation and feldspar alteration. The high amounts of aluminite at the Aroma fan site rather indicate that feldspar weathering is likely to be induced by sufficient meteoric water over time, mobilising Al from the feldspars in the presence of calcium sulphate.

In contrast to the subsurface wedges, the surface crust mineralogy is dominated by gypsum with low contents of clastic minerals, anhydrite, and other evaporites such as aluminite, konyaite, and celestine. The presence of sulphates reflects minor dissolution and reprecipitation of salts, but due to the low content of β-anhydrite and the other sulphates, these processes are less significant than in the subsurface wedge system. However, mineral phases such as celestine were only found as microscopic crystals in the crust's base sample, accompanied with

https://doi.org/10.5194/egusphere-2024-592
Preprint. Discussion started: 15 April 2024
© Author(s) 2024. CC BY 4.0 License.

an increased content of β-anhydrite (~23 wt%). This pattern could indicate either a dehydration process of gypsum or crystallisation processes following extreme evaporation of highly saline brines (Waele et al. 2017), as β-anhydrite also requires highly saline solutions to precipitate. On the contrary, the absence of halite in the surface crust of the Aroma fan could imply that the highly water-soluble halite was washed out of the crust and migrated downwards to deeper levels during rare rain events. Arens et al. (2021) also described this phenomenon and that soluble salts could be partially leached out of such hyperarid soils. As it is unclear how intense and frequent these rain events may have been at the Aroma fan site, it is not yet possible to predict at what depth in the outcrop halite may occur. The ICP-OES results of the analysed wedge probably show traces of NaCl, but we suspect that the absence of halite or chlorides in the surface crust, which should be generally present in the study area (e.g. Voigt et al., 2020), is due to rain-induced leaching of highly soluble salts to greater depths in the outcrop (>2 m). As the outcrop was exposed to atmospheric processes presumably for weeks to months, a sampling or outcrop bias cannot be fully excluded, although we did not find indications for post-exposure alterations.

5.4 Implications of palaeoclimate and environmental conditions during surface crust formation and wedge growth

The largely internally consistent ^{21}Ne surface exposure ages measured in this study may indicate the end of alluvial deposition and the onset of calcium sulphate accumulation during the Pliocene. Likewise, subsurface haloturbation processes and wedge growth as illustrated in Figure 6 may have commenced that time. Due to the surface crust formation and the associated climatic shift towards even drier conditions and fewer wet periods fostering haloturbation processes, wedge growth could have been attenuated already prior to the development of a considerable crust layer. A shift towards hyperarid conditions is believed to have occurred at the transition to the Holocene at the Andean foreslope (e.g. Jordan et al., 2014). Zinelabedin et al. (2022) presented a first approach to applying feldspar luminescence dating to a calcium sulphate wedge from the Aroma fan outcrop. The widespread equivalent dose distribution likely appeared to indicate several phases of wedge growth and a recent wedge growth activity during the Holocene-Pleistocene boundary, derived from a minimum age model (Zinelabedin et al., 2022). The timing of the last wedge growth activity described by the authors would coincide with the Central Andean Pluvial Event (CAPE) at 13.8–8.5 ka (CAPE II; de Porras et al., 2017) potentially providing sufficient moisture to (re)activate haloturbation processes and wedge formation. However, Zinelabedin et al. (2022) concluded that the wedge stratigraphy is not yet resolved due to low subsampling resolution and that further research is needed to comprise the age of calcium sulphate wedge formation.

Since the investigated outcrop is situated within the summer rain regime (Houston, 2006) prevailing at the Andean foreslope, associated sporadic rain events could provide sufficient moisture to feed haloturbation processes and hence wedge formation in the subsurface. The distance of the outcrop from the Aroma fan site to

https://doi.org/10.5194/egusphere-2024-592
Preprint. Discussion started: 15 April 2024
© Author(s) 2024. CC BY 4.0 License.

the coast and its altitude (outcrop located at ~1630 m a.s.l.) imply that fog advection is less likely to contribute to moisture supply at the Andean foreslope (fog advecting from the Pacific is mainly restricted to altitudes <1200 m a.s.l., Cereceda et al. 2008). Based on plant-specific *n*-alkane data from surface sediments and soil profiles, Mörchen et al. (2021) found that the Aroma fan region was affected by rain rather than fog. The authors concluded that episodes of higher water availability (and vegetation) had previously occurred at the Aroma site. Due to the proximity of the Aroma fan outcrop to the winter/summer rain boundary (see Fig.1; isohyets based on Houston 2006), the outcrop is more sensitive to variations in winter/summer rain. Thus, subtle changes in winter and summer rain could result in significantly more rainfall at this site. The presence of Al-bearing sulphates such as aluminite and celestine (Sr-bearing sulphate) also suggests that sufficient moisture is or was at some point available to initiate leaching of Al and Sr from the minerals, but not as much moisture as is required to remove large quantities of calcium sulphate from the deposits. Calcium sulphate dominance in the Aroma fan deposits indicate that mean annual precipitation is unlikely to have exceeded ~30 mm/year (Rech et al. 2003; 2019).

Polygonal patterned grounds can also be observed on surfaces at the northern and southern rim of the Río Loa Canyon within the hyperarid core of the Atacama Desert (see Fig. 7, cf. Allmendinger and González, 2010; Mohren et al., 2020a) It has not been confirmed yet whether wedge-polygon formation processes are active in this locality. However, the local influence of fog (e.g. Cereceda et al., 2008; Schween et al., 2020) could favour an episodic activity of wedge-polygon formation in this region. Thus, a comparison of wedge-polygon structures from different sites in the Atacama Desert is essential to constrain their formation conditions. Understanding and timing of wedge-polygon-formation under hyperarid conditions may also be important for interpreting wedge-polygon formation in other water-limited environments with similar climatic conditions such as on Mars (see Fig. 7). Due to the correlation of polygonal patterned grounds and the occurrence of ground ice on Mars (e.g. Mangold, 2005), their formation mechanisms have been interpreted as periglacial wedge-polygon formation as described in numerous previous studies (e.g. Mangold et al. 2004; Mangold, 2005; Osterloo et al., 2008; Balme and Gallagher, 2009; Levy et al., 2009, 2010; Hauber et al., 2011; Soare et al., 2014). The presence of salt minerals (e.g. Clark and Van Hart, 1981; Hanley et al., 2012; Bishop, et al., 2014; Ehlmann and Edwards, 2014; Vaniman et al., 2018; Dang et al., 2020) suggests that haloturbation could be another potential mechanism for polygonal patterned ground formation in ground ice-limited regions on Mars (<6 % ground ice mass; Mangold, 2005).

https://doi.org/10.5194/egusphere-2024-592
Preprint. Discussion started: 15 April 2024
© Author(s) 2024. CC BY 4.0 License.

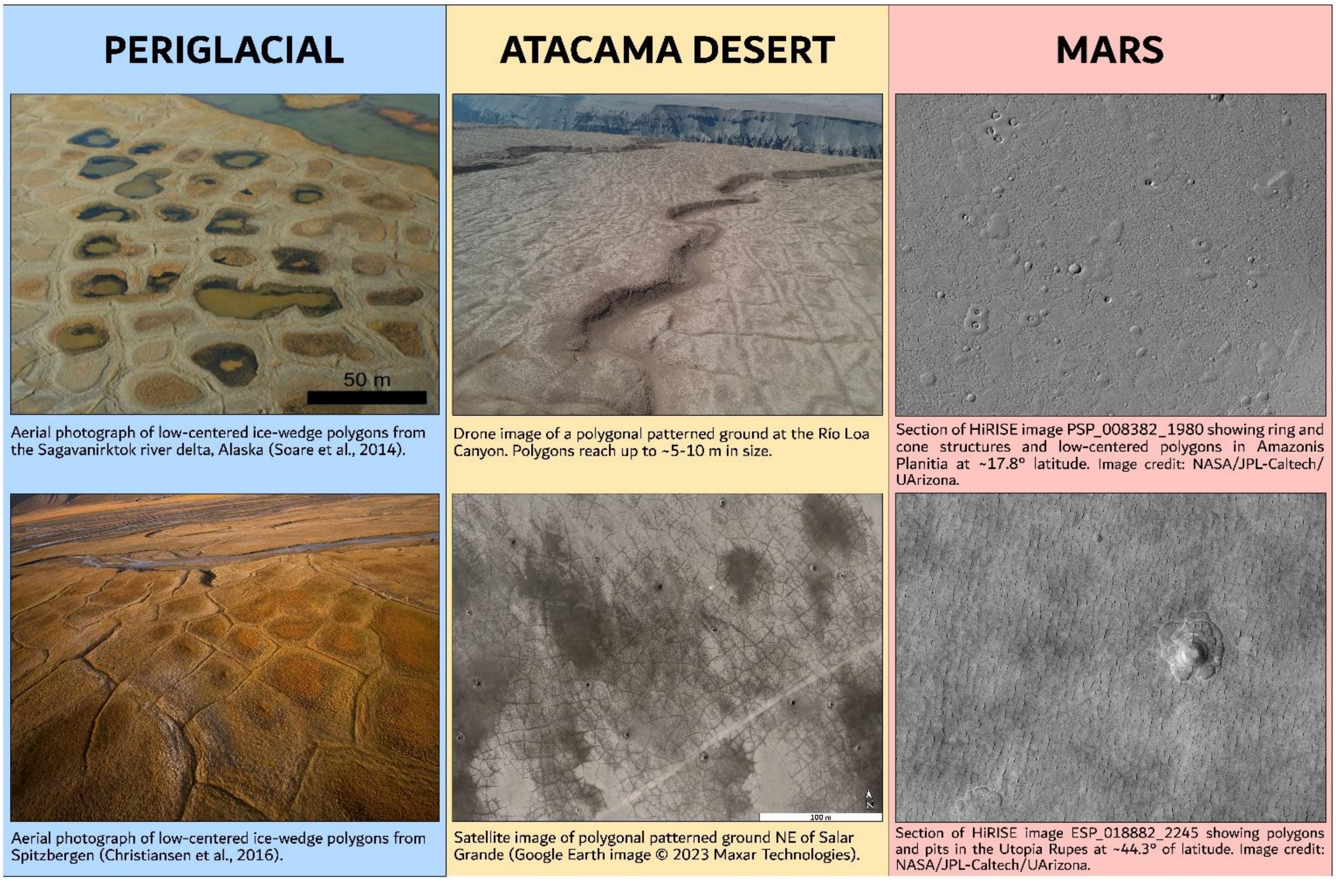

Figure 7: Comparison of different polygonal patterned ground structures from the periglacial region, the Atacama Desert, and the Martian surface. Despite similar appearance of polygonal patterned grounds, formation of these surface structures differs due to different environmental conditions, such as moisture availability, temperature, and the presence of salts in the deposits.

6 Conclusion

The subsurface wedge and soil crack network of the Aroma fan in the northern Atacama Desert is thought to have been predominantly formed by haloturbation processes, dominated by swelling and shrinking processes of calcium sulphate phases. Evidence to support this theory are provided by the high anhydrite content in the vertical wedge laminae and anhydrite-dominated filling of shattered clasts. Since haloturbation and subsurface wedge formation require meteoric moisture from rain events, wedge formation is likely to have occurred under wetter but still (hyper-)arid climatic conditions. Thus, the vertical lamination of the calcium sulphate wedges can potentially be used as a palaeoclimate archive in the Atacama Desert. The calcium sulphate wedge network of the Aroma fan is likely to be associated with a polygonal patterned ground formed at the surface, which was subsequently covered by a gypsum-dominated surface crust. The surface crust is most likely the product of

© Author(s) 2024. CC BY 4.0 License.

long-term net atmospheric deposition of calcium sulphate dust. ^{21}Ne exposure ages obtained from clasts situated on top of the crusts date back to the Pliocene, indicating that the clasts were lifted by the accretionary dust mantle. Long-term accumulation of salts requires a hyperarid climate, which is why we interpret the surface crust to have formed under drier climatic conditions than prevailing when the wedges were formed. Due to this environmental change, we suggest that subsurface wedge and polygonal patterned ground formation may have been attenuated (or stopped), as indicated by the absence of polygonal patterned ground on the surface of the Aroma fan site. While soil fines still appear to be relocated downward inside the surface crust, the bulk of sediments and/or moisture might be mostly retained at the surface over the long term. Further age information from wedge and crust material is required to resolve the timing of the haloturbation processes and the climatic shift towards more hyperarid conditions (crust formation). A comprehensive understanding of wedge-polygon formation by haloturbation under hyperarid conditions could complement wedge-polygon formation hypotheses for other water-limited or hyperarid environments, such as on Mars.

Author contributions

TJD, BR, and AZ conceptualized the study. The project was supervised by TJD and BR. Sample preparation and analyses were performed by AZ. X-ray diffraction measurements were carried out by MWW. Photogrammetry was conducted by JM and AZ. JM performed the preparation of the plutonium samples. SH was responsible for the plutonium measurements. The manuscript was drafted by AZ and internally revised by all authors.

Conflict of Interest

The authors declare that they have no conflict of interest.

Data Availability Statement

All data generated during this study are included in this published article and its supplementary material.

Acknowledgements

This project is affiliated to the Collaborative Research Centre (CRC) 1211 “Earth – Evolution at the Dry Limit” (Grant-No.: 268236062) funded by the German Research Foundation (Deutsche Forschungsgemeinschaft, DFG), Germany. We would like to thank Hanna Cieszynski (University of Cologne) for support with the SEM measurements. We thank Nicole Mantke (University of Cologne) for the performance of the grain size analysis and Jochen Scheld (University of Cologne) for the assistance with the ICP-OES analysis. We would like to thank

© Author(s) 2024. CC BY 4.0 License.

Olympia Nita (University of Cologne) for crushing the XRD samples. Finally, we would like to thank Eduardo Campos and colleagues at the Universidad Católica del Norte in Antofagasta for their logistical assistance during the field campaigns.

References

Alewell, C., Pitois, A., Meusburger, K., Ketterer, M. and Mabit, L.: $^{239+240}$Pu from “contaminant” to soil erosion tracer: Where do we stand?, Earth Sci. Rev., 172, 107–123, doi:10.1016/j.earscirev.2017.07.009, 2017.

Allmendinger, R. W. and González, G.: Invited review paper: Neogene to Quaternary tectonics of the Coastal Cordillera, Northern Chile, Tectonophysics, 495(1–2), 93–110, doi:10.1016/j.tecto.2009.04.019, 2010.

Amit, R., Gerson, R. and Yaalon, D. H.: Stages and rate of the gravel shattering process by salts in desert Reg Soils, Geoderma, 57(3), 295–324, doi:10.1016/0016-7061(93)90011-9, 1993.

Arens, F. L., Airo, A., Feige, J., Sager, C., Wiechert, U. and Schulze-Makuch, D.: Geochemical proxies for water-soil interactions in the hyperarid Atacama Desert, Chile, CATENA, 206, 105531, doi:10.1016/j.catena.2021.105531, 2021.

Balco, G., Stone, J. O., Lifton, N. A. and Dunai, T. J.: A complete and easily accessible means of calculating surface exposure ages or erosion rates from ^{10}Be and ^{26}Al measurements, Quat. Geochronol., 3(3), 174–195, doi:10.1016/j.quageo.2007.12.001, 2008.

Balme, M. R. and Gallagher, C.: An equatorial periglacial landscape on Mars, Earth Planet. Sci. Lett., 285(1–2), 1–15, doi:10.1016/j.epsl.2009.05.031, 2009.

Beaugnon, F., Quiligotti, S., Chevreux, S. and Wallez, G.: On the monoclinic distortion of β-anhydrite $CaSO_4$, Solid State Sci., 108, 106399, doi:10.1016/j.solidstatesciences.2020.106399, 2020.

Benavente, D., Linares-Fernández, L., Cultrone, G. and Sebastián, E.: Influence of microstructure on the resistance to salt crystallisation damage in brick, Mater. Struct., 39(1), 105–113, doi:10.1617/s11527-005-9037-0, 2006.

Bishop, J. L., Quinn, R. and Dyar, M. D.: Spectral and thermal properties of perchlorate salts and implications for Mars, Am. Min., 99(8–9), 1580–1592, doi:10.2138/am.2014.4707, 2014.

Black, R. F.: Periglacial features indicative of permafrost: Ice and soil wedges, Quat. Res., 6(1), 3–26, doi:10.1016/0033-5894(76)90037-5, 1976.

Bobst, A. L., Lowenstein, T. K., Jordan, T. E., Godfrey, L. V., Ku, T.-L. and Luo, S.: A 106ka Paleoclimate record from drill core of the Salar de Atacama, Northern Chile, Palaeogeogr. Palaeoclimatol. Palaeoecol., 173(1–2), 21–42, doi:10.1016/s0031-0182(01)00308-x, 2001.

Böhm, C., Reyers, M., Knarr, L. and Crewell, S.: The role of moisture conveyor belts for precipitation in the Atacama Desert, Geophys. Res. Lett., 48(24), doi:10.1029/2021gl094372, 2021.

Bozkurt, D., Rondanelli, R., Garreaud, R. and Arriagada, A.: Impact of warmer Eastern Tropical Pacific SST on the March 2015 Atacama floods, Mon. Weather Rev., 144(11), 4441–4460, doi:10.1175/mwr-d-16-0041.1, 2016.

Buck, B. J., Rech, J. A., Howell, M. S., Prellwitz, J. and Brock, A. L.: Salt Heave: A new formation process for patterned ground, Atacama Desert, Chile. Geological Society of America Abstracts with Programs 38, no.7, 520, 2006.

Butscher, C., Breuer, S. and Blum, P.: Swelling laws for clay-sulfate rocks revisited, Bull. Eng. Geol., 77(1), 399–408, doi:10.1007/s10064-016-0986-z, 2018.

Butscher, C., Scheidler, S., Farhadian, H., Dresmann, H. and Huggenberger, P.: Swelling potential of clay-sulfate rocks in tunneling in complex geological settings and impact of hydraulic measures assessed by 3D groundwater modeling, Eng. Geol., 221, 143–153, doi:10.1016/j.enggeo.2017.03.010, 2017.

Cabré, A., Remy, D., Marc, O., Burrows, K. and Carretier, S.: Flash floods triggered by the 15–17th March 2022 rainstorm event in the Atacama Desert mapped from insar coherence time series, Nat. Hazards, 116(1), 1345–1353, doi:10.1007/s11069-022-05707-y, 2022.

Campbell-Heaton, K., Lacelle, D. and Fisher, D.: Ice wedges as winter temperature proxy: Principles, limitations and noise in the $\Delta^{18}O$ records (an example from high Arctic Canada), Quat. Sci. Rev., 269, 107135, doi:10.1016/j.quascirev.2021.107135, 2021.

Cereceda, P., Larrain, H., Osses, P., Farías, M. and Egaña, I.: The spatial and temporal variability of fog and its relation to fog oases in the Atacama Desert, Chile, Atmos. Res., 87(3–4), 312–323, doi:10.1016/j.atmosres.2007.11.012, 2008.

https://doi.org/10.5194/egusphere-2024-592
Preprint. Discussion started: 15 April 2024
© Author(s) 2024. CC BY 4.0 License.

Chamizo, E., García-León, M., Peruchena, J. I., Cereceda, F., Vidal, V., Pinilla, E. and Miró, C.: Presence of plutonium isotopes, ^{239}Pu and ^{240}Pu, in soils from Chile, Nucl. Instrum. Methods Phys. Res. B Nucl. Instrum. Meth. B., doi:10.1016/j.nimb.2011.04.021, 2011.

Christiansen, H. H., Matsuoka, N., Watanabe, T.: Progress in Understanding the Dynamics, Internal Structure and Palaeoenvironmental Potential of Ice Wedges and Sand Wedges. Permafrost and Periglac. Process., 27, 365-376. https://doi.org/10.1002/ppp.1920, 2016.

Chukanov, N. V., Krivoveichev, S. V., Chernyatieva, A. P., Möhn, G., Pekov, I. V., Belakovskiy, D. I., Van, K. V. and Lorenz, J. A.: Vendidaite $Al_2(SO_4)(OH)_3Cl•6H_2O$, a new mineral from La Vendida copper mine, Antofagasta region, Chile, Can. Mineral., 51, 559–568. https://doi.org/10.3749/canmi.51.4.559, 2013.

Clark, B. and van Hart, D. C.: The salts of Mars, Icarus, 45(2), 370–378, doi:10.1016/0019-1035(81)90041-5, 1981.

Cody, R. D. and Hull, A. B.: Experimental growth of primary anhydrite at low temperatures and water salinities, Geology, 8, 505–509, https://doi.org/10.1130/00917613(1980)8<505:EGOPAA>2.0.CO;2, 1980.

Cosentino, N. J. and Jordan, T. E.: $^{87}Sr/^{86}Sr$ of calcium sulfate in ancient soils of hyperarid settings as a paleoaltitude proxy: Pliocene to Quaternary constraints for northern Chile (19.5–21.7°S), Tectonics, 36(1), 137–162, doi:10.1002/2016tc004185, 2017.

Croudace, I. W., Rindby, A. and Rothwell, R. G.: ITRAX: description and evaluation of a new multi-function X-ray core scanner. Geol. Soc. Spec. Publ., 267, 51-63, 2006.

Dang, Y., Zhang, F., Zhao, J., Wang, J., Xu, Y., Huang, T. and Xiao, L.: Diverse polygonal patterned grounds in the Northern Eridania Basin, mars: Possible origins and implications, J. Geophys. Res. Planets, 125(12), doi:10.1029/2020je006647, 2020.

de Porras, M. E., Maldonado, A., De Pol-Holz, R., Latorre, C. and Betancourt, J. L.: Late Quaternary environmental dynamics in the Atacama Desert reconstructed from rodent midden pollen records, J. Quat. Sci., 32(6), 665–684, doi:10.1002/jqs.2980, 2017.

del Río, C., Garcia, J.-L., Osses, P., Zanetta, N., Lambert, F., Rivera, D., Siegmund, A., Wolf, N., Cereceda, P., Larraín, H. and Lobos, F.: ENSO influence on coastal fog-water yield in the Atacama Desert, Chile, Aerosol Air Qual. Res., 18(1), 127–144, doi:10.4209/aaqr.2017.01.0022, 2018.

Dewald, A., Heinze, S., Jolie, J., Zilges, A., Dunai, T., Rethemeyer, J., Melles, M., Staubwasser, M., Kuczewski, B., Richter, J., Radtke, U., von Blanckenburg, F. and Klein, M.: CologneAMS, a dedicated center for accelerator mass spectrometry in Germany, Nucl. Instrum. Methods Phys. Res. B Nucl. Instrum. Meth. B., 294, 18–23, doi:10.1016/j.nimb.2012.04.030, 2013.

Diederich, J. L., Wennrich, V., Bao, R., Büttner, C., Bolten, A., Brill, D., Buske, S., Campos, E., Fernández-Galego, E., Gödickmeier, P., Ninnemann, L., Reyers, M., Ritter, B., Ritterbach, L., Rolf, C., Scheidt, S., Dunai, T. J. and Melles, M.: A 68 ka precipitation record from the hyperarid core of the Atacama Desert in northern Chile, Glob. Planet. Change, 184, 103054, doi:10.1016/j.gloplacha.2019.103054, 2020.

Dunai, T. J., González López, G. A. and Juez-Larré, J.: Oligocene–Miocene age of aridity in the Atacama Desert revealed by exposure dating of erosion-sensitive landforms, Geology, 33(4), 321, doi:10.1130/g21184.1, 2005.

Edelman, C. H., Florschutz, F. and Jeswiet, J.: Über Spätpleistozäne und frühholozäne kryoturbate Ablagerungen in östlichen Niederlanden. Verhandelingen van het Geologisch-Mijnbouwkundig Genootschap voor Nederland en Koloniën, Geol. Ser., 11(4), 301–336, 1936.

Ehlmann, B. L. and Edwards, C. S.: Mineralogy of the Martian surface, Annu. Rev. Earth Planet. Sci., 42(1), 291–315, doi:10.1146/annurev-earth-060313-055024, 2014.

Ericksen, A. G. E.: Geology and Origin of the Chilean Nitrate Deposits, Geological Survey Professional Paper, 1188, 1981.

Ericksen, A. G. E.: The Chilean Nitrate Deposits: The origin of the Chilean nitrate deposits, which contain a unique group of saline minerals, has provoked lively discussion for more than 100 years, Am. Sci., 71, 366–374, 1983.

Evenstar, L. A., Hartley, A. J., Stuart, F. M., Mather, A. E., Rice, C. M. and Chong, G.: Multiphase development of the Atacama planation surface recorded by cosmogenic ^{3}He exposure ages: Implications for uplift and Cenozoic climate change in western South America, Geology, 37(1), 27–30, doi:10.1130/g25437a.1, 2009.

© Author(s) 2024. CC BY 4.0 License.

Evenstar, L. A., Mather, A. E., Hartley, A. J., Stuart, F. M., Sparks, R. S. J. and Cooper, F. J.: Geomorphology on geologic timescales: Evolution of the Late Cenozoic pacific paleosurface in northern Chile and Southern Peru, Earth-Sci. Rev., 171, 1–27, doi:10.1016/j.earscirev.2017.04.004, 2017.

Ewing, S. A., Sutter, B., Owen, J., Nishiizumi, K., Sharp, W., Cliff, S. S., Perry, K., Dietrich, W., McKay, C. P. and Amundson, R.: A threshold in soil formation at Earth's arid–hyperarid transition, Geochim. Cosmochim. Acta, 70(21), 5293–5322, doi:10.1016/j.gca.2006.08.020, 2006.

Finstad, K., Pfeiffer, M., McNicol, G., Barnes, J., Demergasso, C., Chong, G. and Amundson, R.: Rates and geochemical processes of soil and salt crust formation in Salars of the Atacama Desert, Chile, Geoderma, 284, 57–72, doi:10.1016/j.geoderma.2016.08.020, 2016.

Flatt, R. J., Caruso, F., Sanchez, A. M. and Scherer, G. W.: Chemo-mechanics of salt damage in stone, Nat. Commun., 5(1), doi:10.1038/ncomms5823, 2014.

Fookes, P. G. and Lee, E. M.: The engineering geology of Playas, Salt Playas and Salinas Q. J. Eng. Geol. Hydrogeol., 51(2), 287–298, doi:10.1144/qjegh2017-084, 2018.

Garreaud, R. D., Vuille, M., Compagnucci, R. and Marengo, J.: Present-day South American climate, Palaeogeogr. Palaeoclimatol. Palaeoecol., 281(3–4), 180–195, doi:10.1016/j.palaeo.2007.10.032, 2009.

Hanley, J., Chevrier, V. F., Berget, D. J. and Adams, R. D.: Chlorate salts and solutions on Mars, Geohys. Res. Lett., 39(8), doi:10.1029/2012gl051239, 2012.

Hardie, L. A.: The gypsum-anhydrite equilibrium at one atmosphere pressure. Amer. Mineral., 52(1-2), 171–200, 1967.

Hartley, A. J. and Evenstar, L.: Cenozoic stratigraphic development in the North Chilean forearc: Implications for basin development and uplift history of the Central Andean Margin, Tectonophysics, 495(1–2), 67–77, doi:10.1016/j.tecto.2009.05.013, 2010.

Hartley, A. J. and May, G.: Miocene gypcretes from the Calama Basin, Northern Chile, Sedimentology, 45(2), 351–364, doi:10.1046/j.1365-3091.1998.0166e.x, 1998.

Hauber, E., Reiss, D., Ulrich, M., Preusker, F., Trauthan, F., Zanetti, M., Hiesinger, H., Jaumann, R., Johansson, L., Johnsson, A., Van Gasselt, S. and Olvmo, M.: Landscape evolution in Martian mid-latitude regions: Insights

https://doi.org/10.5194/egusphere-2024-592
Preprint. Discussion started: 15 April 2024
© Author(s) 2024. CC BY 4.0 License.

from analogous periglacial landforms in Svalbard, Geol. Soc. Spec. Publ., 356(1), 111–131, doi:10.1144/sp356.7, 2011.

Houston, J.: Variability of precipitation in the Atacama Desert: Its causes and hydrological impact, International J. Clim., 26(15), 2181–2198, doi:10.1002/joc.1359, 2006.

Howell, M. S., Buck, B. J., Rech, J. A., Brock, A. L., Prellwitz, J.: Genesis of the Hyperarid Soils of the Atacama Desert: Analogue for Mars?, 18th World Congress of Soil Science, Philadelphia, Pennsylvania, 2006.

Howell, M. S.: Mineralogy and micromorphology of an Atacama Desert soil, Chile: A model for hyperarid pedogenesis, Master's thesis, UNLV Theses, Dissertations, Professional Papers, and Capstones 52, http://dx.doi.org/10.34870/1363798, 2009.

Jarzyna, A., Bąbel, M., Ługowski, D. and Vladi, F.: Petrographic record and conditions of expansive hydration of anhydrite in the recent weathering zone at the abandoned Dingwall Gypsum Quarry, Nova Scotia, Canada, Minerals, 12(1), 58, doi:10.3390/min12010058, 2021.

Joeckel, R. M., Wally, K. D., Ang Clement, B. J., Hanson, P. R., Dillon, J. S. and Wilson, S. K.: Secondary minerals from extrapedogenic *per latus* acidic weathering environments at geomorphic edges, Eastern Nebraska, USA, Catena, 85(3), 253–266, https://doi.org/10.1016/j.catena.2011.01.01, 2011.

Jordan, T. E., Herrera L., C., Godfrey, L. V., Colucci, S. J., Gamboa P., C., Urrutia M., J., González L., G. and Paul, J. F.: Isotopic characteristics and paleoclimate implications of the extreme precipitation event of March 2015 in Northern Chile, Andean Geol., 46(1), 1, doi:10.5027/andgeov46n1-3087, 2019.

Jordan, T. E., Kirk-Lawlor, N. E., Blanco, N. P., Rech, J. A. and Cosentino, N. J.: Landscape modification in response to repeated onset of hyperarid paleoclimate states since 14 Ma, Atacama Desert, Chile, Geol. Soc. Am. Bull., 126(7–8), 1016–1046, doi:10.1130/b30978.1, 2014.

Kelley, J. M., Bond, L. A. and Beasley, T. M.: Global distribution of Pu isotopes and ^{237}Np, Sci Total Environ., 237–238, 483–500, doi:10.1016/s0048-9697(99)00160-6, 1999.

Kober, F., Ivy-Ochs, S., Schlunegger, F., Baur, H., Kubik, P. W. and Wieler, R.: Denudation rates and a topography-driven rainfall threshold in northern Chile: Multiple cosmogenic nuclide data and sediment yield budgets, Geomorphology, 83(1–2), 97–120, doi:10.1016/j.geomorph.2006.06.029, 2007.

https://doi.org/10.5194/egusphere-2024-592
Preprint. Discussion started: 15 April 2024
© Author(s) 2024. CC BY 4.0 License.

Kohl, C. P. and Nishiizumi, K.: Chemical isolation of quartz for measurement of in-situ -produced cosmogenic nuclides, Geochim. Cosmochim. Acta, 56(9), 3583–3587, doi:10.1016/0016-7037(92)90401-4, 1992.

Lachenbruch, A. H.: Mechanics of thermal contraction cracks and ice-wedge polygons in permafrost. Geol. Soc. Am. Spec. Pap., 70, https://doi.org/10.1130/SPE70, 1962.

Lal, D.: Cosmic Ray labeling of erosion surfaces: In situ nuclide production rates and erosion models, Earth Planet. Sci. Lett., 104(2–4), 424–439, doi:10.1016/0012-821x(91)90220-c, 1991.

Latorre, C., González, A. L., Quade, J., Fariña, J. M., Pinto, R. and Marquet, P. A.: Establishment and formation of fog-dependent *tillandsia landbecki i*dunes in the Atacama Desert: Evidence from radiocarbon and stable isotopes, J. Geophys. Res. Biogeosci., 116(G3), doi:10.1029/2010jg001521, 2011.

Levy, J., Head, J. and Marchant, D.: Thermal contraction crack polygons on Mars: Classification, distribution, and climate implications from HiRISE Observations, J. Geophys. Res., 114(E1), doi:10.1029/2008je003273, 2009.

Levy, J., Head, J. W. and Marchant, D. R.: Concentric crater fill in the northern mid-latitudes of Mars: Formation processes and relationships to similar landforms of glacial origin, Icarus, 209(2), 390–404, doi:10.1016/j.icarus.2010.03.036, 2010.

Lifton, N., Sato, T. and Dunai, T. J.: Scaling in situ cosmogenic nuclide production rates using analytical approximations to atmospheric cosmic-ray fluxes, Earth Planet. Sci. Lett., 386, 149–160, doi:10.1016/j.epsl.2013.10.052, 2014.

Liu, X. and Lai, Z.: Optical dating of sand wedges and ice-wedge casts from Qinghai Lake area on the northeastern Qinghai-Tibetan Plateau and its palaeoenvironmental implications, Boreas, 42(2), 333–341, doi:10.1111/j.1502-3885.2012.00288.x, 2012.

Mackay, J. R.: Some observations on the growth and deformation of epigenetic, Syngenetic and anti-syngenetic ice wedges, Permafr. Periglac. Process., 1(1), 15–29, doi:10.1002/ppp.3430010104, 1990.

Mangold, N., Maurice, S., Feldman, W. C., Costard, F. and Forget, F.: Spatial relationships between patterned ground and ground ice detected by the Neutron Spectrometer on Mars, J. Geophys. Res., 109(E8), doi:10.1029/2004je002235, 2004.

Mangold, N.: High latitude patterned grounds on Mars: Classification, distribution and Climatic Control, Icarus, 174(2), 336–359, doi:10.1016/j.icarus.2004.07.030, 2005.

Medialdea, A., May, S. M., Brill, D., King, G., Ritter, B., Wennrich, V., Bartz, M., Zander, A., Kuiper, K., Hurtado, S., Hoffmeister, D., Schulte, P., Gröbner, M., Opitz, S., Brückner, H. and Bubenzer, O.: Identification of humid periods in the Atacama Desert through hillslope activity established by infrared stimulated luminescence (IRSL) dating, Glob. Planet. Change, 185, 103086, doi:10.1016/j.gloplacha.2019.103086, 2020.

Michalski, G., Böhlke, J. K. and Thiemens, M.: Long term atmospheric deposition as the source of nitrate and other salts in the Atacama Desert, Chile: New evidence from mass-independent oxygen isotopic compositions, Geochim. Cosmochim. Acta, 68(20), 4023–4038, doi:10.1016/j.gca.2004.04.009, 2004.

Milsch, H., Priegnitz, M. and Blöcher, G.: Permeability of gypsum samples dehydrated in Air, Geophys. Res. Lett., 38(18), doi:10.1029/2011gl048797, 2011.

Mohren, J., Binnie, S. A., Rink, G. M., Knödgen, K., Miranda, C., Tilly, N. and Dunai, T. J.: A photogrammetry-based approach for soil bulk density measurements with an emphasis on applications to cosmogenic nuclide analysis, Earth Surf. Dyn., 8(4), 995–1020, doi:10.5194/esurf-8-995-2020, 2020a.

Mörchen, R., Amelung, W., Giese, C., Böhnert, T., Ruhm, J. and Lehndorff, E.: Fingerprint of plant life in the Atacama Desert – insights from *n-alkane* analyses, Org. Geochem., 151, 104145, doi:10.1016/j.orggeochem.2020.104145, 2021.

Mossop, G. D. and Shearman, D. J.: Origins of secondary gypsum, Trans. Inst. Mining, Metal. 82, 147-154, 1973.

Muñoz, R. C., Quintana, J., Falvey, M. J., Rutllant, J. A. and Garreaud, R.: Coastal clouds at the eastern margin of the Southeast Pacific: Climatology and trends, J. Clim., 29(12), 4525–4542, doi:10.1175/jcli-d-15-0757.1, 2016.

Neal, J. T., Langer, A. M., Kerr, P. F.: Giant desiccation polygons of Great Basin Playas, Geol. Soc. Am. Bull. 79, 69-90, https://doi.org/10.1130/0016-7606(1968)79[69:GDPOGB]2.0.CO;2, 1968.

Nishiizumi, K., Caffee, M. W., Finkel, R. C., Brimhall, G. and Mote, T.: Remnants of a fossil alluvial fan landscape of Miocene age in the Atacama Desert of northern Chile using cosmogenic nuclide exposure age dating, Earth Planet. Sci. Lett., 237(3–4), 499–507, doi:10.1016/j.epsl.2005.05.032, 2005.

https://doi.org/10.5194/egusphere-2024-592
Preprint. Discussion started: 15 April 2024
© Author(s) 2024. CC BY 4.0 License.

Opel, T., Meyer, H., Wetterich, S., Laepple, T., Dereviagin, A. and Murton, J.: Ice wedges as archives of winter paleoclimate: A Review, Permafr. Periglac. Process., 29(3), 199–209, doi:10.1002/ppp.1980, 2018.

Osterloo, M. M., Hamilton, V. E., Bandfield, J. L., Glotch, T. D., Baldridge A. M., Christensen, P. R., Tornabene, L. L. and Anderson, F. S.: Chloride-bearing materials in the Southern Highlands of Mars. Science 319(5870), 1651–1654, https://doi.org/10.1126/science.115069, 2008.

Placzek, C. J., Matmon, A., Granger, D. E., Quade, J. and Niedermann, S.: Evidence for active landscape evolution in the hyperarid atacama from multiple terrestrial cosmogenic nuclides, Earth Planet. Sci. Lett., 295(1–2), 12–20, doi:10.1016/j.epsl.2010.03.006, 2010.

Placzek, C., Granger, D. E., Matmon, A., Quade, J. and Ryb, U.: Geomorphic process rates in the central Atacama Desert, Chile: Insights from cosmogenic nuclides and implications for the onset of hyperaridity, Am. J. Sci., 314(10), 1462–1512, doi:10.2475/10.2014.03, 2014.

Rech, J. A., Currie, B. S., Jordan, T. E., Riquelme, R., Lehmann, S. B., Kirk-Lawlor, N. E., Li, S. and Gooley, J. T.: Massive Middle Miocene Gypsic Paleosols in the Atacama Desert and the formation of the Central Andean rain-shadow, Earth Planet. Sci. Lett., 506, 184–194, doi:10.1016/j.epsl.2018.10.040, 2019.

Rech, J. A., Currie, B. S., Michalski, G. and Cowan, A. M.: Neogene climate change and uplift in the Atacama Desert, Chile, Geology, 34(9), 761, doi:10.1130/g22444.1, 2006.

Rech, J. A., Quade, J. and Hart, W. S.: Isotopic evidence for the source of Ca and s in soil gypsum, anhydrite and calcite in the Atacama Desert, Chile, Geochim. Cosmochim. Acta, 67(4), 575–586, doi:10.1016/s0016-7037(02)01175-4, 2003.

Reyers, M., Boehm, C., Knarr, L., Shao, Y. and Crewell, S.: Synoptic-to-regional-scale analysis of rainfall in the Atacama Desert (18°–26°S) using a long-term simulation with WRF, Mon. Weather Rev., 149(1), 91–112, doi:10.1175/mwr-d-20-0038.1, 2021.

Ritter, B., Diederich-Leicher, J. L., Binnie, S. A., Stuart, F. M., Wennrich, V., Bolten, A. and Dunai, T. J.: Impact of $CaSO_4$-rich soil on Miocene surface preservation and Quaternary sinuous to meandering channel forms in the hyperarid Atacama Desert, Scientific Reports, 12(1), doi:10.1038/s41598-022-22787-9, 2022.

https://doi.org/10.5194/egusphere-2024-592
Preprint. Discussion started: 15 April 2024
© Author(s) 2024. CC BY 4.0 License.

Ritter, B., Stuart, F. M., Binnie, S. A., Gerdes, A., Wennrich, V. and Dunai, T. J.: Neogene fluvial landscape evolution in the hyperarid core of the Atacama Desert, Scientific Reports, 8(1), doi:10.1038/s41598-018-32339-9, 2018.

Ritter, B., Wennrich, V., Medialdea, A., Brill, D., King, G., Schneiderwind, S., Niemann, K., Fernández-Galego, E., Diederich, J., Rolf, C., Bao, R., Melles, M. and Dunai, T. J.: Climatic fluctuations in the hyperarid core of the Atacama Desert during the past 215 ka, Scientific Reports, 9(1), doi:10.1038/s41598-019-41743-8, 2019.

Ritterbach, L. and Becker, P.: Temperature and humidity dependent formation of $CaSO_4 \cdot XH_2O$ (x = 0...2) phases, Glob. Planet. Change, 187, 103132, doi:10.1016/j.gloplacha.2020.103132, 2020.

Rodriguez-Navarro, C. and Doehne, E.: Salt weathering: influence of evaporation rate, supersaturation and crystallization pattern, Earth Surf. Process. Landf. 24, 191- 209, https://doi.org/10.1002/(SICI)1096-9837(199903)24:3<191::AID-ESP942>3.0.CO;2-G, 1999.

Sager, C., Airo, A., Arens, F. L. and Schulze-Makuch, D.: Eolian erosion of polygons in the Atacama Desert as a proxy for hyper-arid environments on Earth and beyond, Scientific Reports, 12(1), doi:10.1038/s41598-022-16404-y, 2022.

Sager, C., Airo, A., Arens, F. L. and Schulze-Makuch, D.: New type of sand wedge polygons in the salt cemented soils of the hyper-arid Atacama Desert, Geomorphology, 373, 107481, doi:10.1016/j.geomorph.2020.107481, 2021.

Sanzeni, A., Colleselli, F., Crippa, F. and Merlini, M.: On the swelling behaviour of weak rocks due to gypsum crystallization, Procedia Eng., 158, 128–133, doi:10.1016/j.proeng.2016.08.417, 2016.

Schiro, M., Ruiz-Agudo, E. and Rodriguez-Navarro, C.: Damage mechanisms of porous materials due to in-pore salt crystallization, PRL, 109(26), doi:10.1103/physrevlett.109.265503, 2012.

Schween, J. H., Hoffmeister, D. and Löhnert, U.: Filling the observational gap in the Atacama Desert with a new network of climate stations, Glob. Planet. Change, 184, 103034, doi:10.1016/j.gloplacha.2019.103034, 2020.

Soare, R. J., Conway, S. J. and Dohm, J. M.: Possible ice-wedge polygons and recent landscape modification by “wet” periglacial processes in and around the Argyre impact basin, Mars, Icarus, 233, 214–228, doi:10.1016/j.icarus.2014.01.034, 2014.

© Author(s) 2024. CC BY 4.0 License.

Starke, J., Ehlers, T. A. and Schaller, M.: Tectonic and climatic controls on the spatial distribution of denudation rates in northern Chile (18°S to 23°S) determined from cosmogenic nuclides, J. Geophys. Res., 122(10), 1949–1971, doi:10.1002/2016jf004153, 2017.

Stone, J. O.: Air pressure and cosmogenic isotope production, J. Geophys. Res., 105(B10), 23753–23759, doi:10.1029/2000jb900181, 2000.

Stuut, J.-B. W. and Lamy, F.: Climate variability at the southern boundaries of the Namib (southwestern Africa) and Atacama (northern Chile) coastal deserts during the last 120,000 yr., Quat. Res., 62(3), 301–309. https://doi:10.1016/j.yqres.2004.08.001, 2004.

Tang, Y., Gao, J., Liu, C., Chen, X. and Zhao, Y.: Dehydration pathways of gypsum and the rehydration mechanism of soluble anhydrite γ-$CaSO_4$, ACS Omega, 4(4), 7636–7642, doi:10.1021/acsomega.8b03476, 2019.

Tucker, R. M.: Giant polygons in the Triassic salt of Cheshire, England. A thermal contraction model for their origin, J. Sediment. Res., 51, 779–786. https://doi.org/10.1306/212F7DA6-2B24-11D7-8648000102C1865D, 1981.

Vaniman, D. T., Martínez, G. M., Rampe, E. B., Bristow, T. F., Blake, D. F., Yen, A. S., Ming, D. W., Rapin, W., Meslin, P.-Y., Morookian, J. M., Downs, R. T., Chipera, S. J., Morris, R. V., Morrison, S. M., Treiman, A. H., Achilles, C. N., Robertson, K., Grotzinger, J. P., Hazen, R. M., Wiens, R. C. and Sumner, D. Y.: Gypsum, bassanite, and anhydrite at Gale Crater, Mars, Am. Min., 103(7), 1011–1020, doi:10.2138/am-2018-6346, 2018.

Vicencio Veloso, J. M.: Analysis of an extreme precipitation event in the Atacama Desert on January 2020 and its relationship to humidity advection along the Southeast Pacific, Atmósfera, doi:10.20937/atm.52911, 2022.

Voigt, C., Klipsch, S., Herwartz, D., Chong, G. and Staubwasser, M.: The spatial distribution of soluble salts in the surface soil of the Atacama Desert and their relationship to hyperaridity, Glob. Planet. Change, 184, 103077, doi:10.1016/j.gloplacha.2019.103077, 2020.

Wang, F., Michalski, G., Seo, J. and Ge, W.: Geochemical, isotopic, and mineralogical constraints on atmospheric deposition in the hyper-arid Atacama Desert, Chile, Geochim. Cosmochim. Acta, 135, 29–48, doi:10.1016/j.gca.2014.03.017, 2014.

https://doi.org/10.5194/egusphere-2024-592
Preprint. Discussion started: 15 April 2024
© Author(s) 2024. CC BY 4.0 License.

Wang, F., Michalski, G., Seo, J.-H., Granger, D. E., Lifton, N. and Caffee, M.: Beryllium-10 concentrations in the hyper-arid soils in the Atacama Desert, Chile: Implications for arid soil formation rates and El Niño driven changes in Pliocene precipitation, Geochim. Cosmochim. Acta, 160, 227–242, doi:10.1016/j.gca.2015.03.008, 2015.

Washburn, A. L.: Classification of patterned ground and review of suggested origins, Geol. Soc. Am. Bull., 67, 823–865, https://doi.org/10.1177/0309133312438909, 1956.

Washburn, A. L.: Geocryology. A Survey of Periglacial Processes and Environments. ix + 406 pp., numerous illustrations, London: Edward Arnold, ISBN 0713161191, 1979.

Wehmann, N., Lenting, C. and Jahn, S.: Calcium sulfates in planetary surface environments, Glob. Planet. Change, 230, 104257, doi:10.1016/j.gloplacha.2023.104257, 2023.

Wells, S. G., McFadden, L. D., Poths, J. and Olinger, C. T.: Cosmogenic ^{3}He surface-exposure dating of stone pavements: Implications for landscape evolution in deserts, Geology, 23(7), 613-616. https://doi.org/10.1130/0091-7613(1995)023<0613:CHSEDO>2.3.CO;2, 1995.

Wennrich, V., Böhm, C., Brill, D., Carballeira, R., Hoffmeister, D., Jaeschke, A., Kerber, F., Maldonado, A., May, S. M., Olivares, L., Opitz, S., Rethemeyer, J., Reyers, M., Ritter, B., Schween, J. H., Sevinç, F., Steiner, J., Walber-Hellmann, K. and Melles, M.: Late Pleistocene to modern precipitation changes at the Paranal Clay Pan, central Atacama Desert, Glob. Planet. Change, 233, 104349, doi:10.1016/j.gloplacha.2023.104349, 2024.

Williams, G. E.: Precambrian permafrost horizons as indicators of Palaeoclimate, Precambrian Res., 32(2–3), 233–242, doi:10.1016/0301-9268(86)90008-2, 1986.

Winkler, E. M. and Singer, P.: Crystallisation pressure of salts in stone and concrete, Geol. Soc. Am. Bull., 83(11), 3509–3514. https://doi.org/10.1130/0016-7606(1972)83[3509:CPOSIS]2.0.CO;2, 1972.

Zinelabedin, A., Riedesel, S., Reimann, T., Ritter, B. and Dunai, T. J.: Testing the potential of using coarse-grain feldspars for post-IR IRSL dating of calcium sulphate-wedge growth in the Atacama Desert, Quat. Geochronol., 71, 101341, doi:10.1016/j.quageo.2022.101341, 2022.